Journal Pre-proofs

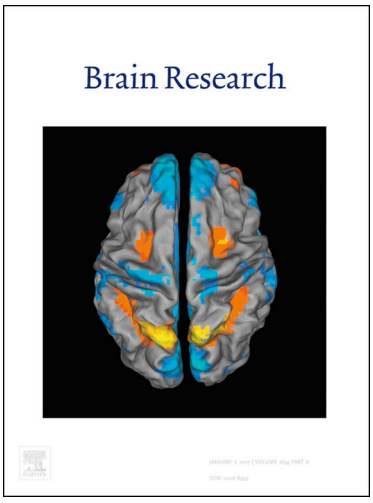

Research paper

Early divergent modulation of NLRP2′s and NLRP3′s inflammasome sensors *vs*. AIM2′s one by signals from Aβ •Calcium-sensing receptor complexes in human astrocytes

Anna Chiarini, Ubaldo Armato, Li Gui, Meifang Yin, Shusen Chang, Ilaria Dal Prà

PII: S0006-8993(24)00537-7
DOI: https://doi.org/10.1016/j.brainres.2024.149283
Reference: BRES 149283

To appear in: *Brain Research*

Received Date: 19 July 2024
Revised Date: 4 October 2024
Accepted Date: 14 October 2024

Please cite this article as: A. Chiarini, U. Armato, L. Gui, M. Yin, S. Chang, I. Dal Prà, Early divergent modulation of NLRP2′s and NLRP3′s inflammasome sensors *vs*. AIM2′s one by signals from Aβ •Calcium-sensing receptor complexes in human astrocytes, *Brain Research* (2024), doi: https://doi.org/10.1016/j.brainres.2024.149283

Early divergent modulation of NLRP2's and NLRP3's inflammasome sensors *vs.* AIM2's one by signals from Aβ•Calcium-sensing receptor complexes in human astrocytes

Anna Chiarini[1]*, Ubaldo Armato[1], Li Gui[2], Meifang Yin[1], Shusen Chang[1], Ilaria Dal Prà[1]*

[1] Department of Surgery, Dentistry, Pediatrics, and Gynecology, University of Verona, 8 Strada Le Grazie, 37134 Verona, Italy.

uarmato@gmail.com (U.A.); meifang.yin@univr.it (M.Y.); 13511848567@163.com (S.C)

[2] Department of Neurology, Southwest Hospital, Third Military Medical University, 29 Gaotanyan Street, Chongqing, 400038, China.

2079244086@email.szu.edu.cn (L.G.)

* Correspondence: A.C., anna.chiarini@univr.it; I.D.P., ilaria.dalpra@univr.it

Abstract

Alzheimer's disease (AD), the most prevalent human dementia, is driven by accruals of extracellular $A\beta_{42}$ senile patches and intracellular neurofibrillary tangles of hyperphosphorylated Tau (p-Tau) proteins. AD's concurrent neuroinflammation is prompted by innate immunity-related cytosolic protein oligomers named inflammasomes. Upon proper "first" (priming) and "second" (activating) signals, inflammasomes overproduce proinflammatory Interleukin (IL)-1β, and IL-18 while cleaving pyroptosis-promoting Gasdermin D's N-terminal fragments. Our earlier studies highlighted that in pure monocultures, exogenous $A\beta_{25-35}$-treated nonproliferating human cortical astrocytes (HCAs) made and released surpluses of endogenous $A\beta_{42}$-oligomers (-os) and p-Tau-os, just as alike-treated human cortical neurons did. $A\beta_{25-35}$-exposed HCAs also over-released NO, VEGFA, and IL-6. Aβ•CaSR (Aβ•Calcium-Sensing Receptor) complexes generated intracellular signals mediating all such neurotoxic effects since CaSR's negative allosteric modulators (aka NAMs or calcilytics, e.g., NPS2143) fully suppressed them. However, it had hitherto remained unexplored whether signals from Aβ•CaSR complexes also induced the early expression and/or activation of NOD-like 2 (NLRP2) and 3 (NLRP3) and of PYHIN absent in melanoma 2 (AIM2) inflammasomes in monocultured HCAs. To clarify this topic, we used *in-situ*-Proximity Ligation, qRT-PCR, double antibody arrays, immunoblots, and Caspase 1/4 enzymatic assays. Aβ•CaSR complexes quickly assembled on HCAs surface and issued intracellular signals activating Akt and JAK/STAT axes. In turn, the latter upregulated NLRP2 and NLRP3 PRRs (pattern recognition receptors) yet downregulated AIM2. These effects were specific, being significantly hindered by NPS2143 and inhibitors of PI3K (LY294002), AMPKα (Dorsomorphin), mTOR (Torin1), and JAK/TYK (Brepoticinib). A wide-spectrum inhibitor, Bay11-7082, intensified the Aβ•CaSR/Akt/JAK/STAT axis-driven opposite control of NLRP3's and AIM2's PRR proteins without affecting NLRP2 PRR upregulation. However, the said effects on the PRRs proteins vanished within 24-h. Moreover, Aβ•CaSR signals neither concurrently changed ASC, pro-IL-1β, and Gasdermin-D (holo- and fragments) protein levels and Caspases 1 and 4 enzymatic activities nor induced pyroptosis. Therefore, Aβ•CaSR cues acted as "first (priming) signals" temporarily increasing NLRP2 and NLRP3 PRRs expression without activating the corresponding inflammasomes. The neatly divergent modulation of NLRP3's *vs*. AIM2's PRR proteins by Aβ•CaSR cues and by Bay11-7082 suggests that, when bacterial or viral DNA fragments are absent, AIM2 might play "anti-inflammasomal" or other roles in HCAs. However, Bay11-7082's no effect on NLRP2 PRR overexpression also reveals that CaSR's downstream mechanisms controlling inflammasomes' sensors are quite complex in HCAs, and hence, given AD's impact on human health, well worth further studies.

Keywords: human astrocytes; NLRP2; NLRP3; AIM2; amyloid-β; calcium-sensing receptor

1. Introduction

Alzheimer's disease (AD), the most prevalent human dementia, occurs mostly as a multifactorial late-onset or sporadic ailment in which genes (e.g., APOEε4, TREM2, and others) play only predisposing roles. Conversely, specific genetic mutations cause the rare (1-3%) early-onset familial AD (Alzheimer's disease facts and figures, 2024). Asymptomatic AD's course lasts from 20 to 40 years, but symptoms (amnesias, cognitive loss, inability to cope) manifest only in the last stage. Unluckily, no AD-modifying therapy is yet available. Concerning AD's pathogenesis, the "amyloid cascade" hypothesis (Haas and Selkoe, 2007; Selkoe and Hardy, 2016) posits that Amyloid-β_{42} ($A\beta_{42}$) oligomer surpluses are its prime drivers. Healthy neurons produce and release from their axon terminals pM amounts of $A\beta_{42}$ monomers (Cirrito et al., 2005), which function as neurotrophic factors safeguarding viability, synaptic' plasticity, and memory storing (Giuffrida et al., 2009; Plant et al., 2003; Puzzo et al., 2008). Age-related failure of various (microglial, vascular, glymphatic) disposal mechanisms and overproduction by neurons and astrocytes cause $A\beta_{42}$ monomers to accrue and congregate first into neurotoxic soluble oligomers ($A\beta_{42}$-os), next into insoluble fibrils, and finally into extracellular senile plaques (Deane et al., 2009; Mawuenyega et al., 2010; Zlokovic et al., 2010). Although senile plaques, which can also release harmful $A\beta_{42}$-os (Bigi et al., 2022), and intracellular Tau protein NFTs (neurofibrillary tangles) are the "core biomarkers" of AD's neuropathology, a concurring third main driver, i.e., neuroinflammation, is needed to bring about dementia (Iwata et al., 2005; Masters and Selkoe, 2012). Notably, various cytosolic innate immunity-related protein oligomers, the inflammasomes, singled out by their specific pattern recognition receptors (PRRs) or sensors, help drive neuroinflammation. In turn, PRRs bind ("sense") three types of molecular patterns (MPs), two of which are endogenous, i.e., damage-associated MPs (DAMPs) and homeostasis-altering MPs (HAMPs), and one is exogenous, i.e., pathogen-associated MPs (PAMPs). The resulting MP•PRR complexes trigger an inflammasome-activating two-signal process. The first signal primes the *de novo* expression of PRRs and of cytokine precursors, i.e., pro-IL-1β and pro-IL-18 (McKee & Coll, 2020; Chen et al., 2021). The second signal (of variable nature) drives the inflammasomes' oligomeric assembly—which includes specific PRRs, ASC (or apoptosis-associated speck-like protein having a Caspase recruitment domain [CARD]) adaptor proteins, and pro-Caspase 1 (inactive cysteine endoprotease)—and canonical activation. Next, self-activated Caspase 1 couples cleave pro-IL-1β and pro-IL-18 into mature IL-1β and IL-18, the extracellular release of which promotes neuroinflammation. From Gasdermin D (GSDMD) holoprotein active Caspase 1 also cleaves N-terminal fragments, which form membrane pores releasing K^+ ions. The resulting ion imbalance promotes the inflammatory death (or pyroptosis) of neural cells. Once evoked by secreted IL-1β and IL-18 and various other factors, a too-intense and/or long-lasting neuroinflammation becomes a dangerously harmful pathological process (Chiarini et al., 2020a).

Astrocytes are the most abundant human brain cell type (Araque and Navarrete, 2010). Astrocytes' physiologically upkeep brain homeostasis, as they form gap-junction-interconnected networks, team up with neuron groups, support crucial metabolic exchanges with their neuron team-mates, wrap up and insulate tripartite synapses, and help keep blood-brain barrier working integrity, (Giaume et al.,2010; Halassa and Haydon, 2010). Traditional views held that astrocytes did not make any Aβ peptides (Aβs) but swept up and degraded those let off from adjacent live or dead neurons (Nielsen et al., 2009). However, once exposed to exogenous fibrillar (f) or soluble (s) $A\beta_{25\text{-}35}$ in separate *in vitro* monocultures, which acted as AD's early-stage preclinical models ("*in a Petri dish*"), nontumorigenic human cortical astrocytes (HCAs) made and secreted surpluses of endogenous $A\beta_{42}$/$A\beta_{42}$-os. This was the result of the activation of APP (amyloid precursor protein)'s neurotoxic amyloidogenic pathway activation at the expense of APP's neurotrophic and neuroprotective nonamyloidogenic pathway (Armato et al., 2013; Chiarini et al., 2017a). Moreover, exogenous $A\beta_{25\text{-}35}$-treated HCAs concurrently made surpluses of AD-like hyperphosphorylated Tau-oligomers (p-Tau-os) and extracellularly released them inside exosomes (Chiarini et al., 2017b). Hence, just like neurons, HCAs can make both $A\beta_{42}$-os and p-Tau-os. In parallel, Aβ-exposed HCAs produced and secreted surfeits of nitric oxide (NO), vascular endothelial growth factor A (VEGFA), IL-6, and various other cytokines/chemokines revealing their gaining of a senescence associated secretory phenotype (SASP) (Armato et al., 2013; Dal Prà et al., 2014a; Chiarini et al., 2020b). Stressful stimuli and other factors can induce cellular senescence in HCAs. Senescent HCAs occur in aging brains (Salminen et al., 2011) and in AD and other neurodegenerative diseases brains (Bhat et al., 2012) and support neuroinflammation and cognitive decline (Salas-Venegas et al., 2023).

Our interest in harmful mechanisms evoked by exogenous Aβs led us to investigate Aβ's interaction with the CaSR, a highly conserved and ubiquitously expressed Family C member of G-protein-coupled receptors (GPCRs) (Brown et al., 1995). CaSR's structure entails a bilobed N-terminal domain, named *Venus's flytrap* (VFT), jutting out from the cells' plasma membrane (Silve et al., 2005); an intercalated cysteine-rich domain (CRD); and a heptahelical transmembrane stretch (the 7TM) that is linked to the C-terminal intracellular domain (ICD). VFT-binding cationic ligands (or agonists) include, besides Ca^{2+}, various mono-, di-, and trivalent inorganic ions; amino acids (e.g., phenylalanine; tryptophan); organic polycations (aminoglycoside antibiotics, polyamines) (Bai, 2004); and Aβs (Dal Prà et al., 2014b). Agonist•VFT complexes variously change CaSR's conformation engendering signals that, through CRD and 7TM, reach the ICD, which then binds heterotrimeric $G_{i/o}$, $G_{q/11}$, $G_{12/13}$, or G_s proteins (Breitwieser, 2013). This activates further downstream signaling cascades, including (*i*) protein kinases (Akt, AMPKα, JAK1/2, PKCs, MAPKs); (*ii*) transcription factors (NF-κB, STATs); (*iii*); phospholipases (A2, C, and D); (*iv*) channel-mediated Ca^{2+} influxes, while inhibiting adenylyl cyclase-mediated cyclic AMP synthesis from ATP (Chakravarty et al., 2012). Most important, positive allosteric modulators (PAMs or calcimimetics) and negative allosteric modulators (NAMs or calcilytics) bind 7TM's specific yet partially superimposed pockets and critically intensify or hinder, respectively, the effects evoked by signals from agonist•VFT complexes (Leach et al., 2016; Nemeth, 2002).

In healthy conditions, CaSR works as a calciostat safeguarding systemic extracellular Ca^{2+} ($[Ca^{2+}]_e$). As to the brain, CaSR's ubiquitous expression (Bandyopadhyay et al., 2010) is highest in hippocampal neurons, astrocytes, microglia, and ependymal cells (Yano et al.,2004). Prenatally, CaSR controls neural cells' mitotic activity, differentiation, and migration. Postnatally, CaSR tunes synaptic plasticity, neurotransmitters release, L-amino acid sensing, and K^+ fluxes (Chattopadhyay et al., 1999; Riccardi and Kemp, 2012). But CaSR also plays distinct, even opposite roles in pathological conditions, such as hypoxia/stroke, tumors, and neurodegeneration (Ward et al., 2012).

About AD, in earlier works, we showed that CaSR signals do mediate all the just-mentioned AD-advancing effects elicited by the exposure to exogenous Aβs. Most importantly, short pretreatments of cortical HCAs in pure monocultures with a CaSR's NAM, e.g., NPS2143 or NPS 89636, prior to $Aβ_{25-35}$ addition suppressed all the latter's just-mentioned neurotoxic effects (Armato et al. 2013; Chiarini et al., 2017a, 2017b, 2020b; Dal Prà et al., 2014a).

As to neuroinflammation, CaSR also functions as an avant-garde DAMP-sensing PRR, whose signaling is triggered by surges in extracellular ions released from injured or dead cells. This activated the NOD (nucleotide oligomerization domain)-like receptor protein 3 (NLRP3) inflammasome in mature monocytes and/or macrophages (Rossol et al., 2012; Zhang et al., 2019; Jäger et al., 2020), and in microglia of AD-model animals (see for details Chiarini et al., 2023). Notably, HCAs express various other PRRs besides the CaSR. Among them, NLPR2 predominates, followed in decreasing order by NLRP3, NLRP4, and PYHIN AIM2 (absent in melanoma 2) (Minkiewicz et al., 2013; Walsh et al., 2014). Therefore, in this study, we explored whether an exposure of monocultured senescent HCAs to exogenous $Aβ_{25-35}$ affected the early transcriptional and translational modulation of three distinct PRR/inflammasomes, namely NLRP2, NLRP3, and AIM2, and of their accessory components PYCARD/ASC, Caspases 1, Caspase 4, IL-1β, and GSDMD. To confirm the specific involvement of CaSR signals from Aβ•CaSR complexes, before adding $Aβ_{25-35}$ we briefly treated other HCAs cultures with CaSR NAM NPS2143. We also researched whether signaling axes placed closely downstream from the CaSR, i.e., PI3K/Akt, and JAK/STAT, might mediate the Aβ•CaSR signaling-elicited effects on PRR/inflammasomes in HCAs.

Altogether, our results highlight for the first time that in senescent HCAs Aβ•CaSR signals quickly upregulated the mRNA and protein expression of NLRP2 and NLRP3 PRRs yet also quickly downregulated AIM2 PRR's one. Moreover, Aβ•CaSR signals increased the phospho-active levels of closely downstream components of Akt and JAK/STAT axes (Tfelt-Hansen et al. 2004; Chakravarty et al., 2012; Rybchyn et al. 2019), which in turn mediated the divergent changes in NLRP2 and NLRP3 PRRs *vs*. AIM2 PRR. Again, the specificity of Akt and JAK/STAT axes effects was proven by their total or significant suppression by pre-treatments with NPS2143 or with specific inhibitors of such signaling cascades. Hence, in HCAs, the three PRRs we investigated belong to two distinct groups, NLRP2 and NLRP3 *vs*. AIM2, whose functions, whether

diverse or opposite, need further clarification. Moreover, our results showed that the early Aβ•CaSR cues functioned only as inflammasomes' "first or priming signals" in HCAs monocultures.

2. Materials and Methods

2.1 Bioethics

The present project was approved (Prog. No. CE118CESC) by the Ethical Committee of Verona's University-Hospital Integrated Company. All the HCAs used in the present experiments were bought from an established commercial source. All experiments were conducted according to the guidelines and regulations of Verona's University-Hospital Integrated Company (Verona, Venetia, Italy).

2.2 Culture of HCAs

Frozen HCAs from a commercial source (Cat. No. 1800-5, CoA No. 0002941, ScienCell Research Laboratories, Carlsbad, CA) upon receipt were quickly thawed, cultured, and propagated in ScienCell medium supplemented with FBS (10%$^{v/v}$) and Astrocyte Growth Supplement (all from ScienCell). HCAs stopped growing upon reaching confluence or after incubation in high-calcium (1.8 mM) DMEM fortified with 10%$^{v/v}$ heat-inactivated FBS (Gibco, Thermo Fisher Scientific, Monza, Italy). Under both proliferating and nonproliferating conditions, the HCAs steadily expressed their characteristic markers—i.e., GFAP and glutamine synthase—being phenotypically "locked-in". HCAs were experimentally used only when proliferatively quiescent and not releasing any nitric oxide (NO). HCAs kept expressing the CaSR both when they proliferated and 1.6-fold more intensely ($p < 0.002$) when they became mitotically quiescent in 1.8 mM Ca^{2+} DMEM. However, the actual levels of extracellular Ca^{2+} did not affect HCAs' CaSR expression levels (Dal Prà et al., 2005). The fraction of HCAs with senescence-associated β-galactosidase (SA-β-gal) activity used in this work was about 33 % ± 6 % (mean ± SD; n=4) (Supplementary Fig. 1). Supplementary Table 1 summarizes various biological features that characterize HCAs' SASP.

2.3 Aβ peptides

$A\beta_{25\text{-}35}$ (or GSNKGAIIGLM; Cat. n. 4030205; Bachem AG, Bubendorf, Switzerland), an established $A\beta_{1\text{-}42}$ proxy (Pike et al., 1995), was resuspended in PBS (final concentration 1.5 mM) to form fibrils. Before experimental use, $A\beta_{25\text{-}35}$ fibrillogenesis was checked *via* thioflavin-T tests. The reversemer peptide $A\beta_{35\text{-}25}$ (Cat. n. 4030076, Bachem) was dissolved in the same way as $A\beta_{25–35}$, yet it did not form fibrils and, when given to the HCAs cultures, was ineffective (not shown). Biotinylated $A\beta_{25–35}$ (Cat. no. AS-62451, AnaSpec Inc., Fremont, CA) was used in immunofluorescence experiments and was resuspended in PBS (final concentration 1.5 mM) to form fibrils (Bigi et al., 2022). For *in-situ* Proximity, Ligation Assay (PLA), soluble biotinylated $A\beta_{25–35}$ (AnaSpec Inc.) was dissolved in DMSO (final concentration 1.5 mM). According to substantial body of evidence $A\beta_{25–35}$ shares alike neurotoxic properties with $A\beta_{1\text{-}42}$, both in vitro and in vivo (reviewed in Canet et al., 2023). Of note, at variance with human healthy brains, human AD brains do produce endogenous $A\beta_{25–35}$ (Kubo et al., 2002, 2003; Gruden et al., 2007).

2.5 Experimental protocol

Just as in earlier works (Armato et al. 2013; Chiarini et al., 2017a, 2017b, 2020b; Dal Prà et al., 2014a), we used pure cultures of confluent, nonproliferating senescent HCAs to investigate the neurotoxic effects of

exposure to $A\beta_{25–35}$. At "0-h", a first group of the culture flasks (cell culture density: $4x10^4$ HCAs per square cm) functioned as untreated controls and received a change of fresh medium, while a second group received fresh medium with added soluble or fibrillar $A\beta_{25–35}$ (20 μM; Bachem). This dose is close to that believed to be in contact with the neural cells' plasma membranes of AD patients (Roberts et al., 2017). Exposure of HCAs to $A\beta_{25–35}$ lasted for the whole duration of the experiments (from 1-h to 72-h). Moreover, this dose of $fA\beta_{25–35}$ evokes the most intense and reproducible effects in HCAs (Armato et al. 2013; Chiarini et al., 2017b; Dal Prà et al., 2014a) and other in vitro models (Canet et al., 2023). A third group of flasks was pretreated at "-0.5-h" time with NPS2143 HCl (CAS No. 324523-20-8; Cat. no. HY-10171; from MedChemExpress EU, Sollentuna, Sweden). NPS2143 is a well-established, highly selective, and specific NAM of the CaSR or calcilytic (Riccardi and Kemp, 2012). NPS2143 was dissolved in DMSO and next diluted with the growth medium at a final concentration of 100 nM. At "0-h" experimental time, the NPS2143-added medium was removed, and fresh medium or the $A\beta_{25–35}$-containing medium was added to the flasks. A fourth group of flasks was pretreated for 30-min with inhibitors of signaling molecules placed just downstream from and activated by the CaSR (Tfelt-Hansen et al. 2004; Chakravarty et al., 2012; Rybchyn et al. 2019), used singly (all from MedChemExpress; listed in Table 1), followed by $fA\beta_{25–35}$ administration to assess their effects on the promotion of inflammasomal PRRs expression. At the end of the treatments, cultured HCAs' RNAs, proteins, and growth media were sampled and stored at -80 °C for later analyses or immediate processing.

Table 1. Inhibitors used in the fourth experimental group before adding $fA\beta_{25–35}$

Chemical compound	Target	CAS No.	Final concentration	MedChemExpress Cat. No.
BAY 11-7082 (BAY)	NLRP3 (ATPase region); IκB kinase β; ubiquitin-specific proteases USP7 and USP21	19542-67-7	5 μM	HY-134532
Brepocitinib P-Tosylate (BPC)	JAK1/JAK2/TYK2	2140301-96-6	400 nM	HY-112708A
Dorsomorphin (DOR)	AMPK	866405-64-3	400 nM	HY-13418A
LY294002 (LY)	PI3K	154447-36-6	8 μM	HY-10108
Torin 1 (TOR)	mTOR	1222998-36-8	32 nM	HY-13003

2.6 Imaging of plasma membrane $A\beta_{25-35}$●CaSR complexes via in-situ Proximity Ligation Assay (isPLA)

The *in-situ* proximity ligation assay (*is*PLA) method, developed by Söderberg et al. (2006), was employed to assess the potential interactions between $A\beta_{25-35}$ and CaSR. The $A\beta_{25-35}$•CaSR complexes were revealed by using the Duolink™ *is*PLA kit (Cat. No. DUO92101, Merck) and visualized using 3D digital renderings. After a brief exposure from 5 to 30 min at 37 °C to soluble *biotinylated* $A\beta_{25-35}$ (5.0 μM; Anaspec) HCAs were next fixed in 4%$^{v/v}$ PFA but not permeabilized. After three 5-min washes with PBS, the samples were incubated with the Duolink™ blocking solution (Merck) for 30-min at 37 °C in a preheated humidity chamber. Mouse monoclonal anti-CaSR antibody (RRID: AB_1078365; 2.5 μg mL^{-1}, clone HL1499; Cat. No. C0493; Merck) and rabbit polyclonal anti-biotin antibody (RRID: AB_67327; 5.0 μg mL^{-1}; Cat. No. A150-109A; Bethyl Laboratories, Montgomery, Texas, USA) diluted in Duolink™ antibody diluent were used as primary antibodies and reacted overnight at 4 °C with gentle shaking. The samples were then rinsed with TBS (Tris base 0.01 M, NaCl 0.15 M, pH 7.4) with no detergents to avoid any plasma membrane permeabilization. The *is*PLA samples *plus* and *minus* secondary probes (Merck) for rabbit and mouse immunoglobulins, at 1:5 in Duolink™ Antibody Diluent, were next added and incubated for one hour at 37 °C. After the exposure to antibodies and *is*PLA probes, the samples were incubated sequentially with Duolink™ Hybridization Solution, Ligation Mix, and Amplification Mix (all from Merck). The single-stranded rolling circle amplification products were hybridized to oligonucleotide probes labeled with the red fluorophore Tye624 (λ_{ex} = 594 nm and λ_{em} = 624 nm) by further incubation with Duolink™ Detection Reagents (Merck). The nuclear DNA was next stained with 30 nM DAPI (Merck). The *is*PLA signals appeared as red fluorescent spots. Laser confocal microscopy acquisition and image deconvolution were performed as previously described (Pacchiana et al., 2014). Optimal acquisition conditions were zoom, 3.00; format, 1024 x 1024; pixel size, 0.90 μm x 0.90 μm; Z-stack, 0.210 μm; and pinhole set at 1.0 Airy unit. Deconvolution of 3-D stack pictures was conducted using Huygens Professional software package (version 4.1, Scientific Volume Imaging B.V.; Netherlands). The Image Pro Plus 3D Viewer package (Image-Pro Plus TM, version 7.0, Media Cybernetics, Bethesda, MD) allowed to gain various projections of 3D Maximum Intensity Projection (MIP) renderings of the original *is*PLA pictures.

2.7 Immunofluorescence (IF) detection of endogenous $A\beta_{42}$

HCAs were treated with 20 μM of $fA\beta_{25-35}$ biotinylated at C-terminus (Cat. no. AS-6245; AnaSpec) for 72 hours. Immunofluorescence analysis was carried out as previously described (Armato et al. 2013). HCAs were fixed in paraformaldehyde (PFA) 4%$^{v/v}$ for 30-min at room temperature and incubated overnight at 4 °C with primary mouse monoclonal antibody against endogenous $A\beta_{42}$ (at 1.0 μg mL^{-1}; RRID: AB_972814; clone 8G7, Cat. no. AM00003PU-N, OriGene Technologies GmbH, Herford, Germany;). After three 5-min-PBS washes, the cells were probed with highly cross-adsorbed Alexa Fluor™ 488–labeled (donkey anti-mouse, at 5 μg mL^{-1}; RRID: AB-141607; Cat.no. A-21202) and Alexa Fluor™ 633–labeled (streptavidin, at 2.5 μg mL^{1}; RRID: AB-2313500; Cat.no. S-21375) secondary antibodies (both from Thermo Fisher Scientific) for 60 min at room temperature. The incubation with secondary antibodies was followed by a 10-min incubation with 30 nM 4′,6-diamidino-2-phenylindole dihydrochloride (DAPI, Merck, Italy) to stain DNA. Coverslips were mounted in anti-bleaching medium (Dabco, Merck). After a final wash, the specimens were examined and photographed under a Leica TCS-SP5 AOBS laser confocal microscope (Leica-Microsystem, Wezlar, Germany), equipped with violet (405 nm laser diode), blue (argon. 488 nm), orange (543 nm), and red (633 nm, HeNe laser) excitation laser lines, using a 40x/1.25 NA oil-immersion microscope objective (HCX PL APO 40x 1.25 OIL UV, Leica-Microsystem). Pictures were analyzed with Leica proprietary software. Proper controls with no addition of primary or secondary antibodies were run in parallel.

2.8 Human JAK/STAT and AKT pathways phosphorylation arrays

The Human JAK/STAT Pathway Phosphorylation Array (Cat. no. AAH-JAKSTAT-1, RayBiotech Life Inc., Peachtree Corners, GA) and the Human/Mouse AKT Pathway Phosphorylation Array C1 (Cat. no. AAH-AKT-1, RayBiotech Life Inc.) were used to examine the respective protein activating phosphorylation

profiles in HCAs cell lysates. HCAs were treated with $fA\beta_{25-35}$ (20 μM) ± NPS2143 (100 nM) for 1 hour. Protein extracts were prepared from three experimental groups (i.e., controls, $A\beta_{25-35}$, and NPS2143 + $A\beta_{25-35}$) following the manufacturer's protocols. The protein contents of the samples were quantified by using the Bio-Rad Protein Assay (Cat. No. 500-0006, Bio-Rad). Briefly, equal amounts (100 μg) of protein extracts were then incubated with the antibody array membranes previously treated with Intercept™ TBS blocking buffer (Cat. No. 927-60001, LI-COR GmbH, Bad Homburg, Germany) for 1-h. After overnight incubation at 4 °C, the array membranes were washed and incubated for 2 hours with the RayBio™ Detection Antibody Cocktail. Thereafter, the membranes were washed again and incubated at room temperature for 1-h with 2.0 mL of IRDye™800CW-conjugated goat anti-rabbit, diluted in Intercept™ TBS blocking buffer (1:3000; Cat.no. 926-32211, LI-COR; RRID: AB-621843). The detectable phosphorylated proteins' positive signals were acquired using an Odissey™ (LI-COR) scanner and quantified using Image Studio™ (version 5.2) software. The positive signal intensities from each array were normalized by comparing them to corresponding positive controls (see Supplemental Fig. 2, showing typically developed double antibody arrays, maps, and membranes).

2.9 Western immunoblotting

First, 1.0×10^6 HCAs were seeded in 25 cm^2 flasks and cultured with 4.0 mL of medium. Duplicated flasks were used for each experimental time point in 3 distinct experiments. At selected time points, both untreated and treated HCAs were scraped into cold PBS, sedimented at 200 *g* for 10 min, and the pellets homogenized in T-PER™ tissue protein extraction reagent (Cat. No. 78519, Thermo Fisher Scientific) added with a complete EDTA-free protease and phosphatase inhibitor cocktail (Cat. No. 78441, Thermo Fisher Scientific). The protein contents of the samples were assessed by the Bio-Rad Protein Assay (Cat. No. 500-0006, Bio-Rad). Briefly, equal amounts (10–20 μg) of protein from the lysates were heat-denatured for 10-min at 70 °C in a proper volume of 1 × NuPAGE™ LDS Sample Buffer (Cat. No. NP0007,) supplemented with 1 × NuPAGE™ Reducing Agent (Cat. No. NP0004). Next, the lysates were loaded on a NuPAGE™ 4-12% (Cat. No. NP0321BOX) or 10% Bis-Tris polyacrylamide gel (Cat. No. NP0301BOX) (all from Thermo Fisher Scientific). After electrophoresis in NuPAGE™ MES SDS Running Buffer (Cat. No. NP0002) using the XCell SureLock™ Mini-Cell, proteins were blotted onto nitrocellulose membranes using the iBlot™ Dry Blotting System (all from Thermo Fisher Scientific) and blocked with Intercept™ TBS blocking buffer (Cat. No. 927-60001, LI-COR) for 1 h at room temperature. Next, the membranes were probed overnight at 4 °C with the primary antibodies listed in Table 2. Next incubation steps of the secondary antibodies (see Table 2) were performed for 1-h at room temperature. Intercept™ TBS blocking buffer-0.02%$^{v/v}$ Tween 20 (LI-COR) was used as the diluent for every incubation with primary or secondary antibodies.

The infrared fluorescence signal was detected using the Odyssey™ Infrared Imaging System (LI-COR). The Image Studio™ software (version 5.2 LI-COR) was employed for fluorescence signal analysis and the quantification of specific protein bands in the immunoblots. This enabled to assess the values of their integrated intensity—i.e., the sum of the individual pixel intensity values for a band, minus the product of the average intensity values of the pixels in the background and the total number of pixels enclosed by the area of the band. The data were always normalized to the corresponding loading control (LC; β-actin) to analyze differences among various samples. The integrated intensities of the bands were then divided by that of the control group, which was normalized to the value of 1.0 (i.e., 100%), which enabled to express the data as fold changes *vs*. controls.

Table 2. Antibodies used in WB

Primary Antibody	Host	RRID[1]	Final	Cat. No. & Supplier

		Accession number	**Dilution**	
anti-AIM2 (D5X7K)	rabbit	AB_2798067	1:500	# 12948, Cell Signaling Technology, Danvers, MA
anti-ASC	rabbit	AB_2887938	1:500	# GTX55818, GeneTex Inc., Alton Pkwy Irvine, CA
anti-Caspase 1 (N1N3)	rabbit	AB_10618781	1:500	# GTX101322, GeneTex Inc.
anti- Caspase 4	rabbit	AB_10643965	1.0 µg mL^{-1}	# SAB3500401, Merck
anti- Gasdermin D (1D1	rabbit	AB_3096199	1:5000	# ZRB1274, Merck
anti-NLRP2	rabbit	AB_3096197	1:5000	# ab137569; Abcam, Cambridge, UK
anti-NLRP3	rabbit	AB_3096198	1:1000	# ABF23, Merck
anti- β actin (C4)	mouse	AB_626632	1.0 µg mL	# sc-47778, Santa Cruz Biotechnology, Germany
anti-IL-1β (B122)	Armenian hamster	AB_627791	1:2000	# sc-12742, Santa Cruz Biotechnology
Secondary Antibody				
IRDye™800CW-conjugated anti-rabbit	goat	AB_621843	1:5000	# 926-32211, LI-COR
IRDye™680CW-conjugated anti-mouse	goat	AB_10956588	1:3000	# 926-68070, LI-COR
Biotin-conjugated anti-Armenian hamster	mouse	AB_628480	1:2000	# sc-2791, Santa Cruz Biotechnology

DyLight^{800}-conjugated streptavidin			1:7500	# SAB3500401, LGC Clinical Diagnostics' KPL, USA

[1] Research Resource Identifier

2.10 Assay of Caspase 1 and Caspase 4 enzymatic activities

Caspase 1 and Caspase 4 enzymatic activities were measured in HCAs protein lysates (50-100 μg) by using the specific 7-amido-4-methyl-coumarin (AMC)-conjugated fluorometric substrate acetyl-Tyr-Glu-Val-Asp-AMC (Ac-YEVD-AMC; Cat. No. sc-300160; Lot. No. 2222, Santa Cruz Biotechnology), and 7-amido-4-trifluoro-methyl-coumarin (AFC)-conjugated fluorometric substrate acetyl-Leu-Glu-Val-Asp-AFC (Ac-LEVD-AFC; Cat. No. A2099; Lot. No. 071K2013, Merck), respectively. The reaction buffer consisted of 20 mM HEPES, 5 mM EDTA, 0.2%$^{v/v}$ bovine serum albumin, 10%$^{v/v}$ glycerol, and 10 mM DTT, pH 7.4. Each substrate had a final concentration of 50 μM. After a 2-h incubation at 37 °C the enzymatic activities were fluorometrically measured at excitation λ_{380} nm and emission λ_{460} nm for Caspase 1 and at excitation λ_{400} nm and emission λ_{505} nm for Caspase 4. The results were expressed in arbitrary units calculated as fluorescence values for mg^{-1} protein.

2.11 Quantitative real-time polymerase chain reaction (qRT-PCR)

The expression analysis of *AIM2*, *NLRP2*, *NLPR3*, *PYCARD*, *CASP1*, *CASP4*, *IL1B*, *IL18, GSDMD* genes was conducted via qRT-PCR. Total RNA was isolated from HCAs treated with fA$\beta_{25\text{-}35}$ (20 μM) ± NPS2143 (100 nM) for 1-h, using PureLink™ RNA Mini Kit (Thermo Fisher Scientific) and next reverse transcribed using High-Capacity cDNA Reverse Transcription kit (Thermo Fisher Scientific) according to the manufacturer's instructions. cDNA (5.0 ng) samples from three distinct experiments were amplified (in triplicate) in a reaction volume of 10.0 μL containing the following reagents: 5.0 μL of TaqMan™ Fast Advanced Master Mix (Thermo Fisher Scientific), and 0.5 μL of TaqMan™ Gene expression assay (20x) specific for each gene (Thermo Fisher Scientific) (for details refer to the ID of TaqMan™ Gene expression assay listed in Supplementary Table 2). qRT-PCR was conducted using the 7500 Fast Real-Time PCR System (Thermo Fisher Scientific), with a pre-PCR step of 20s at 95 °C, followed by 40 cycles of 1s at 95 °C and 20s at 60 °C. Samples were amplified with specific primers and probes for each target, and an NTC sample was run in parallel for all targets. Raw data (Ct, cycle threshold) were analyzed using Biogazelle qbase Plus™ qRT-PCR data analysis software (Biogazelle, Zwijnaarde, Belgium). Fold changes were expressed as calibrated normalized relative quantities (CNRQ) with standard errors (SE). The geometric mean of *TBP-HPRT* reference genes values was used for data normalization. The entire process (extraction, retrotranscription, gene expression, and data analysis) was performed by the qPCR-Service at Cogentech S.r.l., Milan, Italy.

2.12 Statistical analysis

Statistical analysis of the data and the graphs drawing were carried out using Graphpad Prism ver. 10.2.0 (335) (Graphpad Software LLC, Boston, MA) and Sigmastat 3.5™ software package (Systat Software, Inc., Richmond, CA). The power calculation was performed with the α set at 0.05, and the obtained values were ≥ 0.8 in all the analyses. The normal distribution of data was assessed using the Shapiro–Wilk test, according to Royston (1995). Next, data were analyzed by one-way *ANOVA* followed by Dunnett's *post hoc* test. Null hypotheses were rejected when $p < 0.05$. Values are presented as mean ± standard deviation of mean (SD) or ± SE. At least three separate experiments were performed in each instance.

3. Results

3.1 Aβ•CaSR complexes quickly assemble at the outer surface of HCAs plasma membranes

We used confluent, nonproliferating senescent HCAs (see Figure S1 and Table S1) in pure cultures to investigate the formation of Aβ•CaSR complexes. The *is*PLA procedure revealed that from 5 to 15 min following the administration of biotinylated soluble $A\beta_{25\text{-}35}$ (5.0 μM) specific $A\beta_{25\text{-}35}$•CaSR complexes assembled at the outer surface of HCAs' nonpermeabilized plasma membranes (Figs. 1A, e, f, and 1B). Such complexes, initially appearing as tiny *puncta*, increased in number, and coalesced into patches up to 15 min (Figs. 1A, e, f, and 1B). Next, their numbers declined due to an active endocytosis (not shown).

Consistent with earlier works (Armato et al. 2013; Chiarini et al., 2017a, 2017b, 2020b; Dal Prà et al., 2014a), the nontumorigenic (aka untransformed) untreated (Ctr) HCAs of the present study did not produce detectable amounts of endogenous $A\beta_{42}$-os (Fig. 1C). But, again in keeping with earlier observations (Armato et al. 2013; Chiarini et al., 2017a, 2017b, 2020b; Dal Prà et al., 2014a), once exposed to exogenous $fA\beta_{25\text{-}35}$ (20 μM) or $sA\beta_{25\text{-}35}$ (5.0 μM) HCAs produced, accumulated, and secreted surpluses of endogenous $A\beta_{42}$-os (Fig. 1C).

3.2 At 1-h Aβ•CaSR signals drive the activation of Akt/mTOR/AMPKα and TYK2/JAK/STATs axes in HCAs

Ligand•CaSR complexes issue signals that activate various downstream signaling axes (Chakravarty et al., 2012). Thus, to reveal any activation of the Akt/mTOR/AMPKα and TYK2/JAK1-2/STATs axes, which are quite closely placed downstream from the CaSR, we challenged specific antibody arrays with protein extracts from HCAs exposed for 1-h to $A\beta_{25\text{-}35}$ ± NPS2143 and from parallel untreated (control) HCAs.

3.2.1 Akt/mTOR/AMPKα axis

Our results showed that Akt, mTOR, and AMPKα were among the proteins that untreated HCAs most intensely expressed. They also showed that 1-h exposure to exogenous $A\beta_{25\text{-}35}$ alone significantly increased over respective controls the activating phosphorylation levels of Akt^{S473} (+35.5%, $p < 0.05$), $mTOR^{S2448}$ (+15.2, $p < 0.05$), and $AMPK\alpha^{T172}$ (+49.7%, $p < 0.001$) (Fig. 2A).

Conversely, a 30-min pretreatment with CaSR NAM (calcilytic) NPS2143 followed by 1-h exposure to $A\beta_{25\text{-}35}$ (henceforth altogether indicated as the *Double Treatment*) kept at controls' values the phosphorylation levels of Akt^{S473}, and $mTOR^{S2448}$, while partially yet significantly stunted the phospho-$AMPK\alpha^{T172}$ increase (+29.7%, $p < 0.01$ *vs*. controls) (Fig. 2A). Thus, these findings showed that signals from Aβ•CaSR complexes did drive an early (by 1-h) phospho-activation of the Akt/mTOR/AMPKα axis in $A\beta_{25\text{-}35}$-exposed HCAs, since the *Double Treatment* fully suppressed it for Akt^{S473} and $mTOR^{S2448}$ yet partially reduced it for $AMPK\alpha^{T172}$.

3.2.2 JAK1-2/TYK2/STATs axis

Untreated HCAs expressed JAK1 and TYK2 kinases more intensely than JAK2. The activating phosphorylation levels of these enzymes increased *vs*. corresponding controls after 1-h exposure to exogenous $A\beta_{25-35}$ (20 μM) alone i.e., $JAK1^{Tyr1022}$ (+21,4%, $p < 0.05$), $JAK2^{Tyr1007/1008}$ (+31.3%, $p < 0.05$), and $TYK2^{Tyr1054}$ (+32.5%, $p < 0.01$), (Fig. 2B). Concurrently, Aβ•CaSR signals increased the activating phosphorylation of the transcription factors $STAT3^{Tyr705}$ (+25.0%, $p < 0.01$), $STAT5^{Tyr694}$ (+26.3%, $p < 0.05$), and $STAT6^{Tyr641}$ (+34.2%, $p < 0.05$) (Fig. 2B). Conversely, in *Double Treatment*-exposed HCAs the activating phosphorylations of JAK1, JAK2, and TYK2 stayed close to their respective untreated control levels ($p > 0.05$ in all instances) (Fig. 2B). Remarkably, the *Double Treatment* also kept at basal values the activating phosphorylation levels of $STAT3^{Tyr705}$, $STAT5^{Tyr694}$, and $STAT6^{Tyr641}$ (Fig. 2B).

Altogether, these findings showed that Aβ•CaSR signals drove the precocious phospho-activation of the JAK1-2/TYK2/STAT3/5/6 axis in HCAs. By suppressing these effects, the *Double Treatment* proved that they were driven by Aβ•CaSR signals.

3.3 Aβ•CaSR signals swiftly (1-h) upregulate NLRP2 and NLRP3 PRRs in HCAs

3.3.1 NLRP2 PRR

Untreated (control) HCAs set into pure *in vitro* cultures most intensely expressed *NLRP2* mRNA, which was already detectable after 27 Ct. A 1-h exposure to exogenous $A\beta_{25-35}$ (20 μM) by itself significantly increased (+31.3%; $p < 0.05$) *NLRP2*'s mRNA expression levels *vs*. untreated controls (Fig. 3A). Conversely, the *Double Treatment* totally suppressed the otherwise Aβ•CaSR signal-evoked surge and kept *NLRP2* PRR's mRNA levels at control levels (Fig. 3A). These results consisted with a fast stimulation of *NLRP2* gene expression triggered by signals from Aβ•CaSR complexes.

NLRP2 was also the most intensely PRR protein untreated (control) HCAs expressed. After 1-h exposure to exogenous $A\beta_{25-35}$ (20 μM) NLRP2 PRR protein levels remarkably peaked, increasing by 14.9-fold ($p < 0.01$) over untreated controls (Ctr). But after 4-h they had declined to 9.1-fold ($p < 0.01$) over controls (Ctr) (Fig. 3B), to reach near basal levels by 18-h and next not changing up to the 48-h (not shown). The *Double Treatment* reduced the 1-h NLRP2 PRR protein's peak overexpression to 10.7-fold ($p < 0.01$) over untreated controls (Ctr) and to -28.2% ($p < 0.05$) *vs*. $A\beta_{25-35}$ alone. Thereafter, the *Double Treatment* did not affect the slowly falling NLRP2 PRR protein levels (Fig. 3B), which like the $A\beta_{25-35}$ alone-treated ones, reached near basal levels by 48-h (not shown).

These findings showed a fully Aβ•CaSR-driven rapid increase in *NLRP2* PRR mRNA expression while other (yet to be figured out) signals, factors, and mechanisms besides Aβ•CaSR signals teamed up to increase the early synthesis and later slow the fall of the NLRP2 PRR protein toward basal levels.

3.3.2 NLRP3 PRR

Untreated HCAs expressed lower *NLRP3* PRR's mRNA basal levels as they needed for detection 35 Ct (cycle threshold) *vs*. NLRP2's 27 cycles (Fig. 4A). However, a 1-h of exposure to exogenous $A\beta_{25-35\ by}$ itself remarkably increased *NLRP3* PRR mRNA levels over controls' (+76.7%; $p < 0.0001$) (Fig. 4A). In contrast, the *Double Treatment* kept NLRP3 PRR mRNA at controls' levels (Fig. 4A). These results consisted with a fast stimulation of *NLRP3* gene expression driven by signals from Aβ•CaSR complexes.

Untreated HCAs also expressed basal levels of NLRP3 PRR's protein (Fig. 4B). After 1-h of exposure to exogenous $A\beta_{25-35}$ (20 μM) alone NLRP3 PRR protein levels had briskly increased by 14.2-fold *vs*. untreated controls ($p < 0.01$) to decline to 4.7-fold ($p < 0.01$) by 4-h (Fig. 4B), subsequently reaching near basal values by 18-h and thereafter staying unchanged from 18-h to 48-h (not shown). However, the *Double Treatment*

halved NLRP3 PRR protein's 1-h peak to 7.3-fold the Ctr levels ($p < 0.01$ *vs*. Ctr; -48.6%, $p < 0.01$ *vs*. $A\beta_{25-35}$ by itself), which from the 2nd hour onwards started falling just like in the $A\beta_{25-35}$ alone-treated samples (Fig. 4B) reaching about control levels by 48-h (not shown). These results showed that besides a fast Aβ•CaSR-driven increase in *NLRP3* gene expression, other (yet to be figured out) signals, factors, and mechanisms cooperated first to briskly increase and next to slow the fall of NLRP3 PRR protein levels.

3.4 Aβ•CaSR signals drive the early downregulation of AIM2 PRR mRNA and protein in HCAs

In vitro untreated HCAs also expressed discrete *AIM2* mRNA amounts (Fig. 5A). Remarkably, 1-h after adding exogenous $A\beta_{25-35}$ (20 μM) *AIM2* mRNA fell to 0.01% of the Ctr levels ($p < 0.001$). Yet, the *Double Treatment* kept *AIM2* mRNA expression levels at 64.0% of the controls' value ($p < 0.01$ *vs*. Ctr and $p < 0.001$ *vs*. Aβ alone-treated specimens) (Fig. 5A). These results consisted of the fast silencing of *AIM2* gene expression and downregulation of its preexisting mRNAs driven by signals from Aβ•CaSR complexes, an effect partially yet significantly prevented by NPS2143 pretreatment.

Untreated HCAs also expressed discrete amounts of AIM2 PRR protein (Fig. 5B). Exposing HCAs to exogenous $A\beta_{25-35}$ by itself drove a slow decline of AIM2 PRR protein levels (by 1-h, -20%, $p < 0.05$ *vs*. controls; from 3-h-to-6-h, -42% $p < 0.001$ *vs*. controls). Conversely, the *Double Treatment* kept AIM2 PRR protein levels at or close to or over basal values. Thus, the *Double Treatment* suppressed Aβ•CaSR signals-evoked downregulatory effects on AIM2 PRR protein (by 3-h, $p < 0.01$ and by 6-h, $p < 0.001$ *vs*. Aβ alone corresponding values) (Fig. 5B).

These findings revealed that negatively modulating *via* NPS2143 the otherwise activated Aβ•CaSR signaling could directly rescue a relevant part (about 2/3) of *AIM2* mRNA levels and keep AIM2 PRR protein at or slightly above untreated control levels.

Overall, these results showed that two oppositely Aβ•CaSR-controlled PRR groups exist in HCAs, i.e. NLRP2 on one side and NLRP3 and AIM2 on the other side.

3.5 Aβ•CaSR signals oppositely control NLRP2's and NLRP3's PRRs vs. AIM2's PRR via two distinct signaling axes in HCAs

We used a set of specific inhibitors of components of the PI3K/Akt/mTOR/AMPKα and TYK2/JAK1-2/STATs axes and a broad-spectrum putatively anti-inflammatory inhibitor to assess whether their activation by Aβ•CaSR signals effectively changed the early (by 1-hr) expression of NLRP2, NLRP3, and AIM2 PRR proteins. Each of these inhibitors was administered for 30-min prior to adding $A\beta_{25-35}$ (20 μM) to HCAs. Untreated (Ctr) and $A\beta_{25-35}$ alone-treated HCAs were run in parallel. One hour later, we sampled the protein extracts from each experimental group to analyze the expression levels of the three PRR proteins under each condition via immunoblotting.

3.5.1 Effects of inhibitor pretreatments on NLRP2 PRR protein expression levels (Fig. 6A)

In keeping with the above findings, exposure to exogenous $A\beta_{25-35}$ by itself increased within 1-h NLRP2 PRR protein levels by 14.9-fold *vs*. untreated controls. Short (30 min.) pretreatments with singly given specific inhibitors lessened by alike degrees the Aβ-driven NLRP2 PRR protein 1-h expression levels, i.e., *LY*294002 (LY; 8.0 μM), an established PI3K inhibitor (Gharbi et al., 2007), to 8.1-fold over controls and by

-45.6% *vs*. $A\beta_{25-35}$ alone; Dorsomorphin (DOR; 400 nM), an AMPKα's inhibitor (Hu et al., 2023), to 7.1-fold over controls and by -52.3% *vs*. $A\beta_{25-35}$ alone; Torin 1 (TOR; 32 nM), an mTOR and mTORC1/mTORC2 complexes inhibitor (Thoreen, et al., 2009), to 9-fold over controls and by -39.6% *vs*. $A\beta_{25-35}$ alone; and the JAK1/JAK2/TYK2-specific inhibitor Brepocitinib (BPC; 400 nM) (Pippis and Yacyshyn, 2021) to 8.1-fold over controls and by -45.6% *vs*. $A\beta_{25-35}$ by itself (Fig. 6A). Surprisingly, BAY 11-7082 (BAY; 5.0 μM), a broad-spectrum putatively anti-inflammatory inhibitor (Lee et al., 2012), increased further the $A\beta_{25-35}$-evoked NLRP2 PRR protein overexpression over controls in HCAs (Fig. 6A).

Therefore, PI3K/Akt/mTOR/AMPKα and JAK1-2/TYK2/STATs axes, which are placed just downstream from the CaSR, partly yet significantly partook to the early (1-h) upregulation of NLRP2 PRR protein expression by Aβ•CaSR signals. Comparatively, these inhibitors were by about 50% more effective than NPS2143 was (cf. Fig. 3B) indicating that under the conditions examined, besides Aβ•CaSR signals, other (yet to be established) factors cross-talked to these two axes to increase or slow the fall of NLRP2 PRR protein levels in Aβ-exposed HCAs (cf. Fig. 3B). Conversely, the broad-spectrum inhibitor BAY did not affect the Aβ-driven early NLRP2 PRR protein overexpression.

3.5.2 Effects of inhibitor pretreatments on NLRP3 PRR protein expression levels (Fig. 6B)

Compared to controls, $A\beta_{25-35}$ by itself increased by 1-h the NLRP3 PRR protein levels by 14.2-fold in HCAs. Just as for NLRP2 PRR protein, LY lessened the Aβ•CaSR-driven upregulation NLRP3 PRR's protein to 9.8-fold *vs*. controls and by -31.0% *vs*. $A\beta_{25-35}$ alone (Fig. 6B). Also, the pretreatment with BPC or DOR or TOR significantly reduced the early NLRP3 PRR protein upregulation occurring in $A\beta_{25-35}$-treated HCAs to 7.5-fold, 6.6-fold, and 8.4-fold, respectively, *vs*. controls and by -47.2%, -53.5%, and -41.0%, respectively, *vs*. Aβ alone (Fig. 6B). By sharp contrast, BAY increased to 22.2-fold *vs*. controls and by +56.3% *vs*. Ab alone the $A\beta_{25-35}$-driven NLRP3 PRR protein expression level in HCAs (Fig. 6B). Hence, the Akt/mTOR/AMPKα axis and the JAK1-2/TYK2/STAT axis played a partial yet relevant role in the Aβ•CaSR-driven upregulation of NLRP3 PRR protein. Comparatively, the tested inhibitors hindered NLRP3 PRR protein expression as effectively as NPS2143 did (cf. Fig. 4B). This showed that under the conditions examined, Aβ•CaSR signals directly regulated NLRP3 PRR protein overexpression through these two axes. Unexpectedly, part of anti-inflammatory BAY remarkably intensified by one or more mechanisms (to be assessed) the Aβ•CaSR signals elicited NLRP3 PRR protein overexpression in HCAs.

3.5.3 Effects of inhibitor pretreatments on AIM2 PRR protein expression levels (Fig. 6C)

With respect to controls, Aβ•CaSR signals within 1-h reduced by -20% *vs*. controls AIM2 PRR protein levels in HCAs (Fig. 6C). Administering BPC, DOR, or TOR left AIM2 PRR protein at the untreated controls' levels while increasing it (+21%) *vs*. Aβ alone. Instead, LY exposure increased AIM2 PRR protein levels by +19% *vs*. controls and by +49% *vs*. $A\beta_{25-35}$ given by itself (Fig. 6C). Conversely, BAY dramatically cut down AIM2 PRR protein levels, i.e., -70% *vs*. controls and -64.7% *vs*. Aβ (Fig. 6C).

Therefore, the inhibitors of the Akt/mTOR/AMPKα axis and the JAK1-2/TYK2/STAT reversed just like NPS2143 did (cf. Fig. 5B), the downregulation AIM2 PRR protein expression otherwise induced by Aβ•CaSR signals, bringing it up to basal levels. Notably, inhibiting the more upstream-placed PI3K elicited a stronger upregulation of AIM2 PRR *vs*. both controls and Ab alone. However, the deep reduction of AIM2 protein levels brought about after 1-h via yet undetermined mechanisms by the broad-spectrum BAY is further evidence that AIM2 PRR's regulation (and role) neatly diverges from those of NLRP2 and NLRP3 PRRs in HCAs.

3.6 Aβ•CaSR signals marginally affect other inflammasome components in HCAs

Notably, besides PRRs, untreated HCAs expressed basal levels of all the other inflammasome components except IL-18.

3.6.1 PYCARD mRNA and ASC protein levels

Aβ•CaSR signals slightly yet insignificantly decreased at 1-h the basal *PYCARD* mRNA expression levels proper of untreated (control) HCAs (Fig. 7A). Conversely, after 1-h the *Double Treatment* reduced (-28.6%: $p < 0.01$, *vs.* Ctr) *PYCARD* mRNA expression levels (Fig. 7A). Consistently, Aβ•CaSR signals did not significantly change basal ASC protein levels (Fig. 7B). On the other hand, only by 6-h the *Double Treatment* decreased the levels of ASC protein *vs*. both untreated controls (-34.3%, $p < 0.05$) and Aβ-treated samples (-32.4%, $p < 0.05$) (Fig. 7B).

3.6.2 Caspase 1 and Caspase 4 mRNAs, proteins, and enzymatic activity levels

Caspase 1. Untreated (control) HCAs expressed basal *CASP1* mRNA levels that, after 1-h, Aβ•CaSR signals, slightly lessened (-19%: $p < 0.05$). Moreover, compared to controls the *Double Treatment* even further lowered (-43.8%: $p < 0.001$) *CASP1* mRNAs levels in HCAs (Fig. 8A).

Despite the early mRNA decreases, Aβ•CaSR signals did not significantly increase *vs*. controls inactive pro-Caspase 1 holoprotein (50 KDa or p50) levels (by 4-h, +23.1%; and by 8-h, +15.7%; $p > 0.05$ in both instances). The *Double Treatment* had no effect except by 8-h when the Caspase 1 p50 level fell (-28.1*%, $p < 0.01$ *vs*. Aβ alone) (Figs. 8B, 8D). Conversely, the active Caspase 1 fragment (20 kDa or p20) levels decreased marginally and similarly ($p > 0.05$) in the *Double Treatment*-exposed HCAs (Figs. 8C, 8D). Consistently, the biochemically assessed levels of Caspase 1 enzymatic activity did not change ($p > 0.05$) between 0-h (Ctr) and 24-h in the *Double Treatment*-subjected HCAs (Fig. 8E).

Altogether, these findings showed that Aβ•CaSR signals neither increased *CASP1* mRNA expression nor enhanced Caspase 1 p20 enzymatic activity. Therefore, despite the transient surges in NLRP2 and NLRP3 PRRs expression levels, these results suggest that no significant inflammasome activation was driven by Aβ•CaSR signals in HCAs.

Caspase 4 (aka Caspase 11). Caspase 4/11 is involved in non-canonical inflammasome activation (Kayagaki et al. 2011). Also, in brain cells under proinflammatory conditions Caspase 4/11 activity increased upstream from Caspase-1 (Kajiwara et al. 2016). Hence, we checked Caspase 4 expression and enzymatic activity levels. Untreated (control) HCAs expressed basal *CASP4* mRNAs levels that increased after 1-h of exposure to Aβ•CaSR signals (+23.5%; $p < 0.05$ *vs*. controls). Conversely, the *Double treatment* decreased after 1-h *CASP4* mRNA levels with respect Aβ-treated (-36.3%, $p < 0.01$) HCAs (Fig. 8F). Consistently, Aβ•CaSR signals transiently increased at 1-h pro-Caspase 4 (50 kDa) holoprotein levels (+51%, $p < 0.01$ *vs*. controls), which thereafter kept falling (by 6-h, -26%, $p < 0.05$ *vs*. Ctr) (Figs. 8G, 8H). But the *Double Treatment* decreased at 1-, 2-, and 6-h HCAs' Caspase 4 holoprotein levels below both control values ($p < 0.05$), and at 1-h and 2-h below Aβ alone-treated ($p < 0.001$) values (Figs. 8G, 8H). Despite such holoprotein changes, Caspase 4 enzymatic activity levels fell between 0-h and 2-h (-30%, $p < 0.05$ *vs*. Ctr's basal values) in $A\beta_{25–35}$ ± NPS2143-treated HCAs (Fig. 8I). Hence, the activity of Caspase 4 too first transiently decreased and later went back to control levels in HCAs despite its Aβ•CaSR signals driven increased expression and its suppression by the *Double Treatment.*

3.6.3 IL1B and IL18 mRNA and precursor protein levels (Fig. 9A, 9B)

To further prove the lack of activation of HCAs' inflammasomes, we assessed the actual levels of two known proinflammatory and pyroptogenic substrates of Caspase 1.

Untreated (control) HCAs expressed basal levels of *IL1B* mRNA that marginally increased after 1-h exposure to Aβ•CaSR signals (+21.3%; $p < 0.05$). Remarkably, 1-h after the onset of the *Double Treatment* *IL1B* mRNA levels had become undetectable by qRT-PCR (after 40 cycles, -99.9%; $p < 0.0001$ *vs*. both untreated and Aβ-treated HCAs) (Fig. 9A).

However, as compared to untreated controls, the intracellular levels of the pro-IL-1β (37 kDa) protein did not significantly ($p > 0.05$) change during the 4 hours following the onset of either kind of treatment (Fig. 9B). These results consisted of the lack of any increases in Caspase 1 and Caspase 4 basal enzymatic activities (cf. Figs. 8C, 8G). They were congruous with our earlier observations that the amount of secreted mature IL-1β was very tiny and that the main proinflammatory cytokines secreted into the growth medium from Aβ-exposed HCAs were IL-6, RANTES, sICAM1, and nor IL-1β or IL-18 (Chiarini et al., 2020b).

On the other hand, *IL18* mRNA and precursor protein were not detected in any of the experimental groups.

3.6.4 GSDMD mRNA and GSDMD *protein expression (Fig.9C, 9D)*

We assayed GSDMD too, a well-known Caspase 1 substrate (Liu et al., 2020). Untreated (control) HCAs expressed basal levels of *GSDMD* mRNA that fell (-25.1%, $p < 0.01$) after 1-h exposure to Aβ•CaSR signals. The *Double Treatment* also elicited at 1-h a decrease in *GSDMD* mRNA (-30.0%, $p < 0.001$ *vs*. controls) (Fig. 9C).

Moreover, the immunoblot analysis of protein extracts from untreated HCAs showed a discrete expression of GSDMD holoprotein (53 kDa). During 6-h after the onset of Aβ•CaSR signals GSDMD holoprotein's levels slightly but insignificantly decreased ($p > 0.05$). The *Double treatment* elicited the same effects as $A\beta_{25-35}$ by itself ($p > 0.05$ at all time points (Fig. 9D). No protein bands attributable to GSDMD N-terminal proteolytic fragments occurred in any of the three experimental groups. Finally, consistent with our earlier findings (Armato et al. 2013; Chiarini et al., 2017a, 2017b, 2020b; Dal Prà et al., 2014a), neither pyroptosis nor any other kind of cell death occurred in HCAs exposed to $A\beta_{25-35}$ alone (not shown). This further proved that under the experimental conditions tested, while downregulating *AIM2* mRNA, Aβ•CaSR signals only induced NLRP2 and NLRP3 PRRs' overexpression, but neither the full activation of the corresponding inflammasomes nor any overproduction of IL-1β and IL-18 nor the proteolysis of GSDMD in HCAs.

4. Discussion

Astrocytes are the most conspicuous human brain's resident cell type (Araque and Navarrete, 2010). Hence, their interplays with neurons, oligodendroglia, microglia, and cells of cerebral vessels are crucial for the upkeeping of brain's physiological functions. Hence their roles in brain disease are quite relevant. Concerning AD, earlier studies revealed that the Aβ•CaSR signals drove the *de novo* synthesis, accumulation, and spread of Aβ-os, p-Taues, NO, VEGFA, and various proinflammatory cytokines in HCAs (Armato et al. 2013; Chiarini et al., 2017a, 2017b, 2020b; Dal Prà et al., 2014a). Our present results extend earlier ones by showing that HCAs actively partake in AD's onset and progression through the signals emitted by their Aβ•CaSR complexes. The latter divergently affect, at both transcriptional and translational levels, three distinct inflammasomal PRRs, namely NLRP2's, NLRP3's on one side, and AIM2's on the other. Although under the

present experimental conditions, a full assembly and activation of NLRP2 and NLRP3 inflammasomes did not obtain, our results suggest that Aβ•CaSR signals may have acted as "first signals". Yet, under the conditions of this study, the activating "second signals" were missing. But, since the HCAs we used showed SASP features, they are still a relevant model for preclinical AD pathophysiology studies (Lye et al., 2019; Ungerleider et al., 2021).

4.1 Aβ•CaSR interactions and signaling.

Aβs are polycationic peptides reacting with various proteoglycans, lipids, and proteins. Thus, Aβs form complexes with integral membrane proteins, i.e., integrins (Bamberger et al., 2003), APP (amyloid precursor protein) (Shaked et al.,2006), PrP^{Sc} (prion protein) (Nygaard et al., 2009), and transmembrane protein 97 (Colom-Cadena et al., 2024). Besides, Aβs bind cell membrane receptors (Rs), such as $p75^{NTR}$ (Chakravarthy et al., 2012), serpin complex-R (Boland et al., 1996), insulin-R (Zhao et al., 2008), NMDA (N-methyl-D-aspartate)-R (Shankar et al., 2007), FPRL1 (formyl peptide R-like-1) (Le et al., 2001), acetylcholine-R (Jürgensen and Ferreira, 2010), RAGE (R for Advanced Glycosylation End products) (Du et al., 2012), and the CaSR (Dal Prà et al., 2014b). Hitherto, no hierarchy of pathophysiological relevance had been set among such integral proteins or Rs. Altogether, our earlier and present results point to the CaSR as one of the most crucial Aβ-Rs as far as AD's pathophysiology is concerned. From a theoretical standpoint, Aβ•Rs complexes might trigger either harmful or protective responses (Ries and Sastre, 2016). However, our results consistently showed that Aβ•CaSR signals elicited a panoply of uniquely neurotoxic (i.e., AD-promoting) outcomes in HCAs, as well as in postnatal human cortical HCN-1A neurons (Armato et al. 2013; Chiarini et al., 2017a, 2017b, 2020b; Dal Prà et al., 2014a).

4.2 Aβ•CaSR signals specifically activate PI3K/Akt/mTOR/AMPKα and TYK2/JAK/STATs axes in HCAs.

Hitherto, the detailed mechanisms controlling PRRs/inflammasomes activation or deactivation in human AD, and the roles (if any) played in it by signals from Aβ•CaSR signals had not been clearly defined. Therefore, we investigated whether in pure cultures of senescent HCAs the early signals issued from exogenous Aβs•CaSR complexes affected the phospho-activation of the PI3K/Akt/mTOR/AMPKα and TYK2/JAK/STATs axes, which are both placed closely downstream from the CaSR (Chakravarty et al., 2012; Rybchyn et al., 2019; Tfelt-Hansen et al., 2004), thereby mediating or partaking in the transcription, translation, and function of three main PRR/inflammasomes, i.e., NLRP2, NLRP3, and AIM2. The observed effects were specific for Aβs•CaSR signals since a short pretreatment with CaSR NAM NPS2143 suppressed them. Indeed, our results showed that Aβ•CaSR complexes issued signals that within 1-h increased the phosphorylations of specific sites known to activate the PI3K/Akt/mTOR/AMPKα and TYK2/JAK/STATs axes. Although abundant Literature involves both the above two signaling axes in animal models of neuroinflammation (Ben Haim et al., 2015; Desale et al., 2021), this is the first observation that Aβ•CaSR signals quickly and specifically activated them both in senescent HCAs. Notably, this was also relevant to our intent to bring to light any connections mediated by the same two signaling axes between Aβs•CaSR signals and inflammasomes in HCAs.

The PI3K/Akt/mTOR/AMPKα axis crucially upholds cellular homeostasis and regulates the mitotic cell cycle, survival, metabolism, autophagy, senescence, inflammation, and apoptosis. As other cell-surface GPCRs do, CaSR regulates this axis primarily through the activation of the PI3Kγ isoform besides stimulating the phospholipase C system to release intracellular Ca^{2+} *via* the accumulation of inositol triphosphate (IP_3) (Canton et al., 2016; Orduña-Castillo et al., 2022). Disruption of this signaling axis promotes Aβs secretion, Tau hyperphosphorylation, and synaptic failure in AD (Desale et al., 2021). On the other hand, the TYK2/JAK/STATs axis partakes in *CASR* gene upregulation (Canaff et al., 2008) and mediates astrocytes' reactivity in aging and neurological disorders, including AD, Parkinson's disease, stroke, multiple sclerosis, Huntington's disease, and amyotrophic lateral sclerosis (Ben Haim et al., 2015; Jain et al., 2021; Qin et al., 2016). The molecular mechanisms involved in the interplay between the CaSR, and TYK2/JAK/STATs are still undefined. GPCRs other than the CaSR activate the JAK/STAT pathway *via* G proteins (i.e., $G\alpha_s$) and

small GTPases (i.e., Rho and Rac) (Liu et al., 2006; Pelletier et al., 2003). Activation of JAK1/2 signal transduction entails the phosphorylation of STAT transcription factors, which dimerize, translocate into the nucleus, bind specific DNA sites, and modulate gene transcription (Jain et al., 2021). Consistently, Aβ•CaSR signals specifically increased the activating phosphorylations of STAT3, STAT5, and STAT6, which may be involved in the presently seen transcriptional changes in inflammasome-related components.

4.3 Aβ•CaSR signals exert divergently affect the expression of NLRP2, NLRP3 PRRs vs. AIM2 PRR in HCAs.

Here as a preliminary notation, it should be stressed that according to our findings, untreated (control) HCAs expressed at transcriptional (mRNAs) and translational (proteins) basal levels of all the components of inflammasomes, i.e. NLRP2, NLRP3, and AIM2 PRRs, ASC, pro-Caspase 1, pro-Caspase 4, pro-IL-1β, and pro-IL-18. However, since no mature IL-1β and IL-18 could be detected, the inflammasome components were in an inactive conformation. As this work explored whether Aβ•CaSR signals evoked HCAs' NLRP2, NLRP3, and AIM2 PRR/inflammasomal responses, we looked at the early changes in mRNA and protein expression of their components. Our results showed for the first time that Aβ•CaSR signals quickly (at 1-h) and similarly upregulated *vs*. controls the mRNA expression levels of *NLRP2* and *NLRP3* genes, as well as of *CASP4* and *IL1B*, while downregulating *AIM2's*.

In relative terms, *NLRP3's* mRNA increase was greater than *NLRP2*'s. However, in absolute terms, given its much higher basal levels, *NLRP2's* mRNA expression was more intense than *NLRP3's*. Most remarkably, increases in both such mRNAs strictly depended upon Aβ•CaSR signals as pretreatment with calcilytic NPS2143 fully prevented them. The transcription-enhancing effects of Aβ•CaSR signals on *NLRP2, NLRP3,* and *CASP4* mRNAs concurred with early (at 1-h) and huge (*vs*. controls) increases in their corresponding proteins. However, the downregulation of the latter 1-h after the *Double Treatment* was significant yet incomplete, at variance with the full suppression of their corresponding mRNAs. Therefore, besides Aβ•CaSR signals, other (to be defined) factors or signals affected the turnovers of NPLR2 and NLRP3 PRR and pro-Caspase 4 proteins. Thus, these observations do not support the occurrence of any activation of the NLRP2 and NLRP3 inflammasomes under the present experimental conditions even though the cells had at their disposal all the necessary components (see also below about this topic).

Hitherto, only fragmentary evidence has been available about the NLRP2 inflammasome's physiological and/or pathological role(s) in the human brain. Minkiewicz et al. (2013) exposed cultured human cortical astrocytes to exogenous ATP—a DAMP that harmed or dead cells let off—, which, via signals from the P2X7 purinergic receptor and the Probenecid-inhibitable Panx-1 channel, drove the NLRP2 inflammasome's assembly and the release of tiny amounts of mature IL-1β. However, untreated human astrocytes in parallel cultures also secreted alike tiny amounts of mature IL-1β. This suggested that preassembled and signaling NLRP2 inflammasomes be a constitutive feature of human astrocytes, promptly taking part in neuroinflammatory reactions, and hence being candidate therapeutic targets. However, up to now, no further evidence has been gained of an active NLRP2 inflammasome in human astrocytes. Only Zhang et al. (2022) reported that in an AD animal model, piriform cortex astrocytes expressed an $A\beta_{42}$-activated NLRP2 inflammasome; conversely, in the same animal model, glucagon-like peptide-1 analogs suppressed NLRP2's activation and attenuated neuroinflammation and cognitive impairment. On the other hand, NLRP2 PRR protein was the most intensely upregulated protein in neural stem cells and in mature neural cells from patients affected by bipolar disorder (Truvé et al., 2020; Vizlin-Hodzic et al., 2017). Ischemic stroke increased an otherwise low NLRP2 expression in C57BL/6J mouse brains and in oxygen-glucose-deprived mouse astrocytes cultured *in vitro,* suggesting a proapoptotic role for NLRP2 (Sun et al., 2016). The tryptophan metabolite Kynurenine drove NLRP2 expression and signaling in mouse hippocampal astrocytes and in chronic stress-exposed depressive mice (Zhang et al., 2020). Conversely, the results of *NLRP2* gene over expression in HEK293T cells and of NLRP2 gene knockout in human monocytic THP-1 cells suggested that NLRP2 hinders the expression of NF-κB-dependent genes otherwise evoked by different stimuli (Bruey et al., 2004). However, NLRP2 gene and NF-κB p65 subunit expression could be reciprocally regulated (Fontalba et al., 2007). Although by complexing with the TBK1 serine/threonine protein kinase NLRP2 tightly controls interferon regulatory factor 3 (IRF3), hindering the expression of interferon-inducible genes involved in the

innate immunity antiviral response (Yang et al., 2018), it is unclear whether this pathway works in human neural cells. Known innate immunity-unrelated NLRP2 activities have been seen concerning $CD34^+$ hemopoietic differentiation into granulocytes, induction of adipocytes from monocytes and mesenchymal stem cells, trophoblastic differentiation of IPSC human granulosa cells, embryo development, and graft-vs-host disease (Chuang et al., 2015; Kufer and Sansonetti, 2011). Therefore, NLRP2 role(s) depends on the cell type and context under study. Consequently, in HCAs, NLRP2 PRR might play a pro-neuroinflammatory role, as well as other relevant yet undefined physio-pathological roles.

Evidence in the Scientific Literature shows that the NLRP3 inflammasome can be activated in both astrocytes and microglia, although microglia's NLRP3 has hitherto been playing the lion's part (Chiarini et al., 2023). In contrast, Gustin et al. (2015) saw low levels of NLRP3, ASC, and IL-1β transcripts and proteins, consisting with the lack of a functional NLRP3 inflammasome in murine astrocytes despite the latter ones' exposure to various agents, including Aβs, which by contrast robustly activated the NLRP3 inflammasome in microglia. On the other hand, postmortem studies showed that the presence of NLRP3, Caspase 8, and cleaved GSDMD concurred with the absence of ASC, Caspase 1, and mature IL-18 in the astrocytes of the middle temporal lobe (Brodmann's area 36) and hippocampus CA1 subfield of AD brains. The authors concluded that in pre-AD and AD brains, astrocyte pyroptosis might be activated through a cell type-specific non-canonical pathway not involving NLRP3 (Moonen et al., 2023). These findings significantly increase our understanding of postmortem AD's neuropathology. However, our present *in vitro* model aimed at investigating the very first HCAs reactions driven by an exposure to $A\beta_{25-35}$ through the signaling of Aβ•CaSR complexes. This amply justifies the divergence of the reported results. At any rate, the inflammasomal regulation is a complex process influenced by a variety of factors that can either keep inflammasomes in a not-expressed or inhibited condition or activate their signals driving the *de novo* production of proinflammatory cytokines and pyroptosis-inducing GSDMD N-terminal fragments (for more details see Chiarini et al. 2023; McKee and Coll, 2020). Consistent with this are the findings of Mészáros et al. (2023), who investigated the NLRP3 inflammasome's role in triple-negative breast cancer (TNBC) brain metastases. They found that healthy human astrocytes did express at detectable levels neither NLRP3 nor IL-1β. Yet, metastatic TNBC cells secreted soluble factors that did upregulate the NLRP3 inflammasome's expression and, via its signals, activated IL-1β synthesis in the same human astrocytes. In keeping with Moonen et al. (2023), it is worth recalling here that inflammasome-controlling mechanisms are highly specific, as they significantly vary between humans and animal species and even among the different viscera or cells of the same organism (Chiarini et al., 2020a, 2023, 2024).

Moreover, the present findings show, for the first time, that Aβ•CaSR signals quickly and deeply downregulated (*vs*. controls) *AIM2's* mRNA expression levels in HCAs. Conversely, blocking Aβ•CaSR signals with an NPS2143 pretreatment proficiently though incompletely preserved *AIM2's* mRNA levels and, particularly after 2-h, AIM2's PRR protein levels. Hence Aβ•CaSR signals divergently regulate AIM2's PRR from NLRP2's and NLRP3's ones. The actual role(s) of AIM2 PRR/inflammasome in human astrocytes and the whole brain is still uncertain. In late-phase EAE (experimental autoimmune encephalomyelitis) astrocytes, AIM2 activation did not induce IL-1β-mediated neuroinflammation but promoted astrogliosis (Barclay et al., 2022). In EAE microglia, Ma et al. (2021) showed an inflammasome-independent function of AIM2 that restrained neuroinflammation by negatively regulating cyclic-GMP-AMP (cGAMP) synthase (cGAS) signaling *via* DNA-PK–AKT3 axis. Besides, in the absence of dsDNA fragments, AIM2 regulated neurons' morphology and affected memory and anxiety in mice (Wu et al., 2016). As our results show that CaSR NAM NPS2143 hindered the downregulation of AIM2 otherwise brought about by $A\beta_{25-35}$, we cannot exclude an anti-inflammatory role for HCAs' AIM2, which, however, requires further assessment.

4.4 Effects of specific inhibitors of signaling axes components on NLRP2, NLRP3, and AIM2 PRRs protein expression.

We also assessed whether the PI3K/Akt/mTOR/AMPKα and TYK2/JAK/STATs signaling axes mediated the Aβ•CaSR signals' effects on the expression of NLRP2, NLRP3, and AIM2 PRR proteins. To this purpose we shortly (30-min) pretreated HCAs with specific inhibitors of members of the said axes prior to adding exogenous $A\beta_{25-35}$. The results proved the tested inhibitors partially yet significantly suppressed the Aβ•CaSR signals-driven increases in NLRP2 and NLRP3 PRR proteins while fully hindering the fall of

AIM2's PRR protein. Since DOR, BPC, and CaSR NAM NPS2143 blocked NLRP3 PRR protein increases with alike intensities, it is likely that Aβ•CaSR signals tightly control NLRP3 PRR protein expression *via* these two axes. Conversely, DM, BPC, LY, and TOR inhibited NLRP2 PRR protein expression more intensely than NPS2143 did. Hence, Aβ•CaSR signals by themselves may exert a weaker inducing effect on NLRP2 PRR protein, which would also be affected by other drivers—a topic requiring further studies. On the other hand, since BCP, DOR, TOR, and LY restored the basal or higher expression levels of AIM2 PRR protein, Aβ•CaSR signals lessened AIM2 PRR's protein levels just *via* the enzymes such inhibitors blocked. In summary, our findings support the view that Aβ•CaSR signals via the PI3K/Akt/mTOR/AMPKα and TYK2/JAK/STATs axes partook in the upregulation of NLRP2's and NLRP3's PRRs and in the downregulation of AIM2's PRR.

Finally, the BAY inhibitor provided a further proof that the mechanisms controlling NLRP2 and NLRP3 proteins levels diverged from those regulating AIM2 PRR protein in HCAs. BAY significantly amplified Aβ•CaSR signals' contrasting effects on both NLRP3 and AIM2 PRRs while did not modify NLRP2's PRR protein level. Albeit BAY inhibits multiple targets, it has been held to act as an anti-inflammatory agent blocking IκB-α phosphorylation, hence NF-κB, and NLRP3 signaling. Yet, BAY also inhibits the ubiquitin-specific proteases USP7 and USP21 (Jiang et al., 2017; Ritorto et al., 2014). Deubiquitinating enzymes crucially control inflammasomes' activation since their chemical inhibition can obstruct NLRP3 inflammasome's oligomerization (Juliana et al., 2012). Moreover, inhibitors of ubiquitin-specific proteases also cause a transient accumulation of ubiquitylated inflammasome components, including PRRs, leading to their degradation at different rates (Lopez-Castejon et al., 2013). Since early BAY's effects in HCAs sharply differed from those it evoked in animal models (Jiang et al., 2017; Liang et al., 2022), they are worthy of further investigation.

4.5 Effects of CaSR NAM NPS2143 on other NLRP2, NLRP3, and AIM2 inflammasome components or substrates.

To assess whether Aβ•CaSR signals drove the assembly and activation of NLRP2 and NLRP3 inflammasomes, an assessment of their effects on other inflammasomal components was in order. Remarkably, our results showed that despite the decrease in *PYCARD* mRNA expression, ASC protein levels were not affected by Aβ•CaSR signals and were only marginally decreased at 3-h and 6-h by the *Double Treatment*. As the latter observation neither excluded nor supported inflammasomes' activation, we assessed the effects of Aβ•CaSR signals on Caspase 1 and on Caspase 4, as the latter plays a crucial role in non-canonical inflammasome activation (Kayagaki et al., 2011). Notably, *CASP1* mRNA levels were decreased by both Aβ•CaSR signals and the *Double Treatment*; yet, despite this, the Caspase 1 protein levels and basal enzymatic activity did not change. Conversely, notwithstanding that Aβ•CaSR signals increased *CASP4* mRNA and protein levels, Caspase 4 basal enzymatic activity remained unchanged.

Although Aβ•CaSR signals modestly increased the expression of *IL1B* gene by 1-h, the *Double Treatment* very deeply suppressed it. Conversely, GSMD mRNA was curtailed by both treatments. However, the intracellular levels of IL-1β precursor protein and of GSMD holoprotein remained at control levels, and mature IL-1β, IL-18, and GSDMD N-terminal fragments could not be detected. These observations consisted with the lack of observed changes in Caspase 1 and Caspase 4 activity.

Therefore, under the conditions of the present study, the Aβ•CaSR signals did not prompt the oligomerization and activation of any of the studied inflammasomes. It follows that the early significant increases in *NLRP2* and *NLRP3*, *CASP4*, and *IL1B* mRNA transcriptions brought about Aβ•CaSR signals stood for a "first (or priming) signal". However, the "second signal" needed for inflammasomes' oligomerization and activation from microglia and/or neurons (Jha et al., 2019; Smith et al., 2022) was absent from the present *in-vitro* model.

From the above discussion, one could infer that the lack of inflammasomes' activation by Aβ•CaSR signals allowed HCAs to survive under the present short-term circumstances. But, given their multiple homeostasis-preserving roles, HCAs survival is a pressing necessity sustained by compensatory mechanisms

that remain mostly to be investigated (Galea et al., 2022). Under long-term situations like AD, HCAs still survive longer than neurons, although they progressively lose functional capabilities while intensifying their neurotoxic roles (Liddlelow et al., 2017; Beretta et al., 2020; Kostantinidis et al., 2023).

5. Conclusions and future perspectives

HCAs and neurons express at their plasma membranes the CaSR, a receptor binding multiple cationic ligands besides Ca^{2+} and functioning as a calciostat, a regulator of crucial cell processes, and a plasma membrane PRR for DAMPs like Aβs and brisk extracellular Ca^{2+} surges (Chiarini et al., 2016, 2020a). Our present results show that the CaSR and exogenous Aβs form complexes, which emit signals bringing about the phospho-activation of the PI3K/Akt/mTOR/AMPKα and TYK2/JAK/STATs signaling axes. The latter partake in the upregulation of NLRP2 and NLRP3 PRRs and in the downregulation of AIM2 PRR. Although not achieving full inflammasome assembly and activation, the same Aβ•CaSR signals drive manifold neurotoxic and also proinflammatory responses (for details, see Fig. 10 and cited references) from HCAs endowed with characteristics proper of the SASP (see Fig. S1 and Table S1) (Simmnacher et al., 2020; López-Teros et al., 2024). The consequently over secreted $Aβ_{42}$-os and p-Taues and several proinflammatory cytokines, including IL-6, could further advance AD's spread *via* the self-sustaining assembly of novel Aβ•CaSR complexes in brain areas newly invaded by the progressive neuropathology (Armato et al., 2013; Chiarini et al., 2017a, 2017b). In this context, the signals from Aβ•CaSR complexes play a significant role by strengthening many features proper of the SASP [i.e., overproduction of VEGFA, IL-6, RANTES, sICAM1, MCP-2, NOS-2/NO (Chiarini et al., 2020b; Dal Prà et al., 2014a), and the phospho-activation of JAK2/STAT3 and mTOR (present work)]. Most remarkably, in a preclinical *in vitro* human AD model, all these neurotoxic effects elicited by Aβ•CaSR signals were fully or significantly prevented by a CaSR NAM (e.g., NPS2143) (Fig. 10). Hence, our previous and present findings entail translational implications by supporting CaSR NAMs as likely modifiers of AD's inexorable course.

Abbreviations

Aβs, amyloid-β peptides

Aβ-os, amyloid-β oligomers

AD, Alzheimer's disease

Akt, protein kinase B

AIM2, absent in melanoma 2 protein

AMPKα, AMP-activated protein kinase α

APP, amyloid precursor protein

ASC, apoptosis-associated speck-like adaptor protein having a CARD

BAY, BAY 11-7082,

BBB, blood-brain barrier

BPC, Brepoticinib

cAMP, cyclic AMP

CaSR, calcium-sensing receptor

CASP1, caspase 1 gene

CASP4, caspase 4 gene

CNRQ, calibrated normalized relative quantity

DAMPs, damage-associated molecular patterns

DOR, Dorsomorphin

Double treatment, NPS2143 (100 nM, 30-min) + $A\beta_{25-35}$ (20 μM)

GPCRs, G-protein-coupled receptors

GSDMD, gasdermin D gene

HAMPs, homeostasis-altering molecular patterns

HCAs, human cortical astrocytes

ICAM-1, intercellular adhesion molecule-1

IF, immunofluorescence

IL, interleukin

is-PLA, *in-situ* proximity ligation assay

JAK, Janus kinase

LC, loading control

LOAD, late onset Alzheimer's disease

LPS, lipopolysaccharide

LY, LY294002

MCP2, monocyte chemotactic protein 2

MPs, molecular patterns

mTOR, mechanistic target of rapamycin

HCAs, nontumorigenic adult human astrocytes

NAM, negative allosteric modulator

NFT, neurofibrillary tangle

NLR, NOD-like receptor

NLRP, nucleotide-binding domain, leucine-rich repeat and PYRIN domain holding protein

NO, nitric oxide

NOD, nucleotide-binding oligomerization domain

NOS-2, nitric oxide synthase-2

NPS, NPS2143

-os, oligomers

p-Tau, hyperphosphorylated Tau protein

p-Tau-os, p-Tau oligomers

PAM, positive allosteric modulator

PAMPs, pathogen-associated molecular patterns

PI3K, phosphoinositide 3-kinase

PRRs, pattern recognition receptors

PYCARD, ASC gene

PYHIN, pyrin and hematopoietic interferon-inducible nuclear domain

R, receptor

RANTES, regulated upon activation, normal T cell expressed and secreted

sAPPα, soluble APPα

sICAM1, soluble ICAM1

SA-βGal, senescence-associated beta-galactosidase

SASP, senescence associated secretory phenotype

STAT, signal transducer and activator of transcription

TYK2, tyrosine Kinase 2

TOR, Torin 1

VEGFA, vascular endothelial growth factor A

WB, western blotting

Funding: This research was funded by the FUR 2022 allotment from the Italian MUR (Ministry of University & Research) to AC and IDP. No funds were provided by private or commercial sources.

Dr. M.Y. is a Ph.D. student at the University of Verona, (Italy) with a fellowship from Shenzhen's University, China.

Dr. S.C. is a fellow at the University of Verona, (Italy) supported by the China Scholarship Council (Scholarship-CSS No. 202208520064).

CRediT authorship contribution statement: Anna Chiarini: Conceptualization, Methodology, Data curation, Formal analysis, Funding acquisition, Investigation, Project administration, Validation, Visualization, Writing—original draft preparation, Writing—review and editing, Supervision. **Ubaldo Armato:** Conceptualization, Data curation, Formal analysis, Writing—original draft preparation, Writing—review and editing, Supervision. **Li Gui:** Data curation, Writing—original draft preparation. **Meifang Yin:** Investigation, Writing—original draft preparation. **Shusen Chang:** Data curation, Writing—original draft preparation. **Ilaria Dal Prà:** Conceptualization, Methodology, Data curation, Formal Analysis, Funding acquisition, Investigation, Project administration, Validation, Visualization, Writing—original draft preparation, Writing—review and editing. All authors have read and approved the final manuscript.

Declaration of competing interest

The authors declare that they have no known competing financial interests or personal relationships that could have appeared to influence the work reported in this paper.

Data availability

Data will be made available on request.

Appendix A. Supplementary data

Supplementary data to this article can be found online at…

References

2024 Alzheimer's disease facts and figures. 2024. Alzheimers Dement. 20(5), 3708-3821. https://doi.org/10.1002/alz.13809.

Araque, A., Navarrete, M., 2010. Glial cells in neuronal network function. Philos. Trans. R. Soc. Lond. B Biol. Sci. 365(1551), 2375–2381. https://doi.org/10.1098/rstb.2009.0313.

Armato, U., Chiarini, A., Chakravarthy, B., Chioffi, F., Pacchiana, R., Colarusso, E., Whitfield, J. F., Dal Prà, I., 2013. Calcium-sensing receptor antagonist (calcilytic) NPS2143 specifically blocks the increased secretion of endogenous Aβ42 prompted by exogenous fibrillary or soluble Aβ25-35 in human cortical astrocytes and neurons-therapeutic relevance to Alzheimer's disease. Biochim. Biophys. Acta 1832(10), 1634-52. https://doi.org/10.1016/j.bbadis.2013.04.020.

Bai, M., 2004. Structure-function relationship of the extracellular calcium-sensing receptor. Cell Calcium 35(3), 197-207. https://doi.org/10.1016/j.ceca.2003.10.018.

Bamberger, M. E., Harris, M. E., McDonald, D. R., Husemann, J., Landreth, G. E., 2003. A cell surface receptor complex for fibrillar beta-amyloid mediates microglial activation. J. Neurosci. 23(7), 2665–74. https://doi.org/10.1523/JNEUROSCI.23-07-02665.2003.

Bandyopadhyay S, Tfelt-Hansen, J., Chattopadhyay, N., 2010. Diverse roles of extracellular calcium-sensing receptor in the central nervous system. J. Neurosci. Res. 88, 2073–82. https://doi.org/10.1002/jnr.22391.

Barclay, W. E., Aggarwal, N., Deerhake, M. E., Inoue, M., Nonaka, T., Nozaki, K., Luzum, N. A., Miao, E. A., Shinohara, M. L., 2022. The AIM2 inflammasome is activated in astrocytes during the late phase of EAE. JCI Insight7(8), e155563. https://doi.org/10.1172/jci.insight.155563.

Ben Haim, L, Ceyzériat, K., Carrillo-de Sauvage, M. A., Aubry, F., Auregan, G., Guillermier, M., Ruiz, M., Petit, F., Houitte, D., Faivre, E., et al., 2015. The JAK/STAT3 pathway is a common inducer of astrocyte reactivity in Alzheimer's and Huntington's diseases. J. Neurosci. 35(6), 2817-29. https://doi.org/10.1523/JNEUROSCI.3516-14.2015.

Beretta, C., Nikitidou, E., Streubel-Gallasch, L., Ingelsson, M., Sehlin, D., Erlandsson, A., 2020. Extracellular vesicles from amyloid-β exposed cell cultures induce severe dysfunction in cortical neurons. Sci Rep 10, 19656. https://doi.org/10.1038/s41598-020-72355-2.

Bhat, R., Crowe, E. P., Bitto, A., Moh, M., Katsetos, C. D., Garcia, F. U., Johnson, F. B., Trojanowski, J. Q., Sell, C., Torres, C., 2012. Astrocyte senescence as a component of Alzheimer's disease. PLoS One 7(9), e45069. https://doi.org/10.1371/journal.pone.0045069.

Bigi, A., Cascella, R., Chiti, F., Cecchi, C. 2022. Amyloid fibrils act as a reservoir of soluble oligomers, the main culprits in protein deposition diseases. Bioessays 44(11), e2200086. https://doi.org/10.1002/bies.202200086

Boland, K., Behrens, M., Choi, D., Manias, K., Perlmutter, D. H., 1996. The serpin-enzyme complex receptor recognizes soluble, nontoxic amyloid-beta peptide but not aggregated, cytotoxic amyloid-beta peptide. J. Biol. Chem. 271(30), 18032–44. https://doi.org/10.1074/jbc.271.30.18032.

Breitwieser, G. E., 2013. The calcium sensing receptor life cycle: trafficking, cell surface expression, and degradation. Best Pract. Res. Clin. Endocrinol. Metab. 27(3), 303-13. https://doi.org/10.1016/j.beem.2013.03.003.

Brown, E. M., Pollak, M., Chou, Y. H., Seidman, C. E., Seidman, J. G., Hebert, S. C., 1995. Cloning and functional characterization of extracellular Ca(2+)-sensing receptors from parathyroid and kidney. Bone 17(2 Suppl), 7S-11S. https://doi.org/10.1016/8756-3282(95)00199-n.

Bruey, J. M., Bruey-Sedano, N., Newman, R., Chandler, S., Stehlik, C., Reed, J.C., 2004. PAN1/NALP2/PYPAF2, an inducible inflammatory mediator that regulates NF-kappaB and caspase-1 activation in macrophages. J. Biol. Chem. 279(50),51897-51907. https://doi.org/10.1074/jbc.M406741200.

Canaff, L, Zhou, X., Hendy, G. N., 2008. The proinflammatory cytokine, interleukin-6, up-regulates calcium-sensing receptor gene transcription via Stat1/3 and Sp1/3. J. Biol. Chem. 283(20), 13586–600. https://doi.org/10.1074/jbc.M708087200.

Canet, G., Zussy, C., Hernandez, C., Maurice, T., Desrumaux, C., Givalois, L., 2023. The pathomimetic oAβ_{25-35} model of Alzheimer's disease: Potential for screening of new therapeutic agents. Pharmacol. Ther. 245,108398. https://doi.org/10.1016/j.pharmthera.2023.108398.

Canton, J., Schlam, D., Breuer, C., Gütschow, M., Glogauer, M., & Grinstein, S., 2016. Calcium-sensing receptors signal constitutive macropinocytosis and facilitate the uptake of NOD2 ligands in macrophages. Nat. Commun. 7, 11284. https://doi.org/10.1038/ncomms11284.

Chakravarthy, B., Gaudet, C., Ménard, M., Brown, L., Atkinson, T., Laferla, F. M., Ito, S., Armato, U., Dal Prà, I., Whitfield, J., 2012a. Reduction of the immunostainable length of the hippocampal dentate granule cells' primary cilia in 3xAD-transgenic mice producing human Aβ(1-42) and tau. Biochem. Biophys. Res. Commun. 427(1), 218–22. https://doi.org/10.1016/j.bbrc.2012.09.056.

Chakravarty, B., Chattopadhyay, N., Brown, E. M., 2012b. Signaling through the extracellular calcium-sensing receptor (CaSR). Adv. Exp. Med. Biol. 740, 103–142. https://doi.org/10.1007/978-94-007-2888-2_5.

Chattopadhyay, N., Ye, C., Yamaguchi, T., Nakai, M., Kifor, O., Vassilev, P. M., Nishimura, R. N., Brown, E. M., 1999. The extracellular calcium-sensing receptor is expressed in rat microglia and modulates an outward K+ channel. J. Neurochem. 72(5), 1915–22. https://doi.org/10.1046/j.1471-4159.1999.0721915.x.

Chen, M. Y., Ye, X. J., He, X. H., & Ouyang, D. Y., 2021. The Signaling Pathways Regulating NLRP3 Inflammasome Activation.Inflammation, 44(4), 1229–1245. https://doi.org/10.1007/s10753-021-01439-6.

Chiarini, A., Armato, U., Liu, D., Dal Prà, I., 2016. Calcium-Sensing Receptors of Human Neural Cells Play Crucial Roles in Alzheimer's Disease. Front. Physiol. 7, 134. https://doi.org/10.3389/fphys.2016.00134.

Chiarini, A., Armato, U., Liu, D., Dal Prà, I., 2017a. Calcium-Sensing Receptor Antagonist NPS2143 Restores Amyloid Precursor Protein Physiological Non-Amyloidogenic Processing in Aβ-Exposed Adult Human Astrocytes. Sci. Rep. 7(1), 1277. https://doi.org/10.1038/s41598-017-01215-3.

Chiarini, A., Armato, U., Gardenal, E., Gui, L., Dal Prà, I., 2017b. Amyloid β-Exposed Human Astrocytes Overproduce Phospho-Tau and Overrelease It within Exosomes, Effects Suppressed by Calcilytic NPS2143-Further Implications for Alzheimer's Therapy. Front. Neurosci. 11, 217. https://doi.org/10.3389/fnins.2017.00217.

Chiarini, A., Armato, U., Hu, P., Dal Prà, I., 2020a. Danger-Sensing/Patten Recognition Receptors and Neuroinflammation in Alzheimer's Disease. Int. J. Mol. Sci. 21(23), 9036. https://doi.org/10.3390/ijms21239036.

Chiarini, A., Armato, U., Hu, P., Dal Prà, I., 2020b. CaSR Antagonist (Calcilytic) NPS2143 Hinders the Release of Neuroinflammatory IL-6, Soluble ICAM-1, RANTES, and MCP-2 from Aβ-Exposed Human Cortical Astrocytes. Cells 9(6), 1386. https://doi.org/10.3390/cells9061386.

Chiarini, A., Gui, L., Viviani, C., Armato, U., Dal Prà, I., 2023. NLRP3 Inflammasome's Activation in Acute and Chronic Brain Diseases-An Update on Pathogenetic Mechanisms and Therapeutic Perspectives with Respect to Other Inflammasomes. Biomedicines 11(4), 999. https://doi.org/10.3390/biomedicines11040999.

Chiarini, A., Armato, U., Gui, L., Dal Prà, I., 2024. “Other Than NLRP3" Inflammasomes: Multiple Roles in Brain Disease. Neuroscientist 30(1), 23-48. https://doi.org/10.1177/10738584221106114.

Chuang, C. Y., Huang, M. C., Chen, H. F., Tseng, L. H., Yu, C. Y., Stone, L., Huang, H. P., Ho, H. N., & Kuo, H. C., 2015. Granulosa cell-derived induced pluripotent stem cells exhibit pro-trophoblastic differentiation potential. Stem Cell Res. Ther. 6(1),14. https://doi.org/10.1186/s13287-015-0005-5.

Cirrito, J.R., Yamada, K. A., Finn, M. B., Sloviter, R. S., Bales, K. R., May, P. C., Schoepp, D. D., Paul, S. M., Mennerick, S., Holtzman, D. M., 2005. Synaptic activity regulates interstitial fluid amyloid-beta levels in vivo. Neuron 48(6), 913-22. https://doi.org/10.1016/j.neuron.2005.10.028.

Colom-Cadena, M., Toombs, J., Simzer, E., Holt, K., McGeachan, R., Tulloch, J., Jackson, R. J., Catterson, J. H., Spires-Jones, M. P., Rose, J., et al., 2024. Transmembrane protein 97 is a potential synaptic amyloid beta receptor in human Alzheimer’s disease. Acta Neuropathol. 147(1), 1-22. https://doi.org/10.1007/s00401-023-02679-6.

Dal Pra, I., Chiarini, A., Nemeth, E. F., Armato, U., Whitfield, J. F., 2005. Roles of Ca2+ and the Ca2+-sensing receptor (CASR) in the expression of inducible NOS (nitric oxide synthase)-2 and its BH4 (tetrahydrobiopterin)-dependent activation in cytokine-stimulated adult human astrocytes. J. Cell. Biochem. 96(2), 428–438. https://doi.org/10.1002/jcb.20511.

Dal Prà, I., Armato, U., Chioffi, F., Pacchiana, R., Whitfield, J. F., Chakravarthy, B., Gui, L., Chiarini, A., 2014a. The Aβ peptides-activated calcium-sensing receptor stimulates the production and secretion of vascular endothelial growth factor-A by normoxic adult human cortical astrocytes. Neuromolecular Med. 16(4), 645-57. https://doi.org/10.1007/s12017-014-8315-9.

Dal Prà, I., Chiarini, A., Pacchiana, R., Gardenal, E., Chakravarthy, B., Whitfield, J. F., Armato, U., 2014b. Calcium-Sensing Receptors of Human Astrocyte-Neuron Teams: Amyloid-β-Driven Mediators and Therapeutic Targets of Alzheimer's Disease. Curr. Neuropharmacol. 12(4), 353-364. https://doi.org/10.2174/1570159X12666140828214701.

Deane, R., Bell, R. D., Sagare, A., Zlokovic, B. V., 2009. Clearance of amyloid-beta peptide across the blood-brain barrier: implication for therapies in Alzheimer's disease. CNS Neurol. Disord. Drug Targets 8(1), 16-30, https://doi.org/10.2174/187152709787601867.

Desale, S. E., Chidambaram, H., Chinnathambi, S., 2021. G-protein coupled receptor, PI3K and Rho signaling pathways regulate the cascades of Tau and amyloid-β in Alzheimer's disease. Mol. Biomed. 2(1), 17. https://doi.org/10.1186/s43556-021-00036-1.

Du, H., Li, P., Wang, J., Qing, X., Li, W., 2012. The interaction of amyloid β and the receptor for advanced glycation endproducts induces matrix metalloproteinase-2 expression in brain endothelial cells. Cell. Mol. Neurobiol. 32(1), 141–7. https://doi.org/10.1007/s10571-011-9744-8.

Fontalba, A., Gutierrez, O., Fernandez-Luna, J. L., 2007. NLRP2, an inhibitor of the NF-kB pathway, is transcriptionally activated by NF-kB and exhibits a nonfunctional allelic variant. J. Immunol. 179:8519–24. https://doi.org/10.4049/jimmunol.179.12.8519

Galea, E., Weinstock, L. D., Larramona-Arcas, R., Pybus, A. F., Giménez-Llort, L., Escartin, C., & Wood, L. B., 2022. Multi-transcriptomic analysis points to early organelle dysfunction in human astrocytes in Alzheimer's disease. Neurobiol. Dis. 166, 105655. https://doi.org/10.1016/j.nbd.2022.105655

Gardenal, E., Chiarini, A., Armato, U., Dal Prà, I., Verkhratsky, A., Rodríguez, J. J., 2017. Increased Calcium-Sensing Receptor Immunoreactivity in the Hippocampus of a Triple Transgenic Mouse Model of Alzheimer's Disease. Front. Neurosci. 11, 81. https://doi.org/10.3389/fnins.2017.00081.

Gharbi, S. I., Zvelebil, M. J., Shuttleworth, S. J., Hancox, T., Saghir, N., Timms, J. F., Waterfield, M. D., 2007. Exploring the specificity of the PI3K family inhibitor LY294002. Biochem. J. 404(1), 15-21. https://doi.org/10.1042/BJ20061489.

Giaume, C., Koulakoff, A., Roux, L., Holcman, D., Rouach, N., 2010. Astroglial networks: a step further in neuroglial and gliovascular interactions. Nat. Rev. Neurosci. 11(2), 87–99. https://doi.org/10.1038/nrn2757.

Giuffrida, M.L., Caraci, F., Pignataro, B., Cataldo, S., De Bona, P., Bruno, V., Molinaro, G., Pappalardo, G., Messina, A., Palmigiano, A., Garozzo, D., Nicoletti, F., Rizzarelli, E., Copani, A., 2009. Beta-amyloid monomers are neuroprotective. J. Neurosci. 29(34), 10582-7. https://doi.org/10.1523/JNEUROSCI.1736-09.2009.

Gruden, M. A, Davidova, T. B., Malisauskas, M., Sewell, R. D., Voskresenskaya, N. I., Wilhelm, K., Elistratova, E. I., Sherstnev, V. V., Morozova-Roche, L. A., 2007. Differential neuroimmune markers to the onset of Alzheimer's disease neurodegeneration and dementia: autoantibodies to Abeta ((25-35)) oligomers, S100b and neurotransmitters. J. Neuroimmunol. 186(1-2), 181-192. https://doi.org/10.1016/j.jneuroim.2007.03.023.

Gustin, A., Kirchmeyer, M., Koncina, E., Felten, P., Losciuto, S., Heurtaux, T., Tardivel, A., Heuschling, P., Dostert, C., 2015. NLRP3 Inflammasome Is Expressed and Functional in Mouse Brain Microglia but Not in Astrocytes. PLoS One10(6), e0130624. https://doi.org/10.1371/journal.pone.0130624.

Haass, C. and Selkoe, D.J., 2007. Soluble Protein Oligomers in Neurodegeneration: Lessons from the Alzheimer's Amyloid ß-Peptide. Nat. Rev. Mol. Cell Biol. 8, 101-112. https://doi.org/10.1038/nrm2101.

Halassa, M. M., Haydon, P. G., 2010. Integrated brain circuits: astrocyte networks modulate neuronal activity and behavior. Annu. Rev. Physiol. 72, 335–55. https://doi.org/10.1146/annurev-physiol-021909-135843.

Hu, Y., Xu, J., Wang, J., Zhu, L., Wang, J., Zhang, Q., 2023. DPP-4 Inhibitors Suppress Tau Phosphorylation and Promote Neuron Autophagy through the AMPK/mTOR Pathway to Ameliorate Cognitive Dysfunction in Diabetic Mellitus. ACS Chem. Neurosci. 14(18), 3335–46. https://doi.org/10.1021/acschemneuro.2c00733.

Iwata, N., Higuchi, M., Saido, T. C., 2005. Metabolism of amyloid-beta peptide and Alzheimer's disease. Pharmacol. Ther. 108(2), 129-48. https://doi.org/10.1016/j.pharmthera.2005.03.010.

Jäger, E., Murthy, S., Schmidt, C., Hahn, M., Strobel, S., Peters, A., Stäubert, C., Sungur, P., Venus, T., Geisler, M., et al., 2020. Calcium-sensing receptor-mediated NLRP3 inflammasome response to calciprotein particles drives inflammation in rheumatoid arthritis. Nat. Commun. 11, 4243. https://doi.org/10.1038/s41467-020-17749-6.

Jain, M., Singh, M. K., Shyam, H., Mishra, A., Kumar, S., Kumar, A., Kushwaha, J., 2021. Role of JAK/STAT in the Neuroinflammation and its Association with Neurological Disorders. Ann. Neurosci. 28(3-4), 191–200. https://doi.org/10.1177/09727531211070532.

Jha, M. K., Jo, M., Kim, J. H., Su, K., 2019. Microglia-Astrocyte Crosstalk: An Intimate Molecular Conversation. Neuroscientist 25(3), 227–40. https://doi.org/10.1177/1073858418783959.

Jiang, W., Li, M., He, F., Zhou, S., Zhu, L., 2017. Targeting the NLRP3 inflammasome to attenuate spinal cord injury in mice. J. Neuroinflammation 14(1), 207. https://doi.org/10.1186/s12974-017-0980-9.

Juliana, C., Fernandes-Alnemri, T., Kang, S., Farias, A., Qin, F., Alnemri, E. S., 2012. Non-transcriptional priming and deubiquitination regulate NLRP3 inflammasome activation. J. Biol. Chem. 287(43), 36617-22. https://doi.org/10.1074/jbc.M112.407130.

Jürgensen, S., Ferreira, S. T., 2010. Nicotinic receptors, amyloid-beta, and synaptic failure in Alzheimer's disease. J. Mol. Neurosci. 40(1-2), 221–9. https://doi.org/10.1007/s12031-009-9237-0.

Kajiwara, Y., McKenzie, A., Dorr, N., Gama Sosa, M. A., Elder, G., Schmeidler, J., Dickstein, D. L., Bozdagi, O., Zhang, B., Buxbaum, J. D., 2016. The human-specific CASP4 gene product contributes to Alzheimer-related synaptic and behavioural deficits. Hum. Mol. Genet. 25(19), 4315-4327. https://doi.org/10.1093/hmg/ddw265.

Kayagaki N, Warming S, Lamkanfi M, Vande Walle L, Louie S, Dong J, Newton K, Qu Y, Liu J, Heldens S, Zhang J, Lee WP, Roose-Girma M, Dixit VM. Non-canonical inflammasome activation targets caspase-11. Nature. 2011 Oct 16;479(7371):117-21. doi: 10.1038/nature10558. PMID: 22002608.

Konstantinidis, E., Dakhel, A., Beretta, C., & Erlandsson, A., 2023. Long-term effects of amyloid-beta deposits in human iPSC-derived astrocytes. Mol. Cell. Neurosci. 125, 103839. https://doi.org/10.1016/j.mcn.2023.103839

Kubo, T., Nishimura, S., Kumagae, Y., Kaneko, I., 2002. In vivo conversion of racemized beta-amyloid ([D-Ser 26]A beta 1–40) to truncated and toxic fragments ([D-Ser 26] A beta 25–35/40) and fragment presence in the brains of Alzheimer's patients. J. Neurosci. Res. 70, 474–483. https://doi.org/10.1002/jnr.10391.

Kubo, T., Kumagae, Y., Miller, C. A., Kaneko, I., 2003. Beta-amyloid racemized at the Ser26 residue in the brains of patients with Alzheimer disease: implications in the pathogenesis of Alzheimer disease J. Neuropathol. Exp. Neurol. 62(2003), 248-259. https://doi.org/10.1093/jnen/62.3.248.

Kufer, T. A., Sansonetti, P. J., 2011. NLR functions beyond pathogen recognition. Nat. Immunol. 12, 121–8. https://doi.org/10.1038/ni.1985.

Le, Y., Gong, W., Tiffany, H. L., Tumanov, A., Nedospasov, S., Shen, W., Dunlop, N. M., Gao, J. L., Murphy, P. M., Oppenheim, J. J., Wang, J. M., 2001. Amyloid (beta)42 activates a G-protein-coupled chemoattractant receptor, FPR-like-1. J. Neurosci. 21(2), RC123. https://doi.org/10.1523/JNEUROSCI.21-02-j0003.2001.

Leach, K., Gregory, K. J., Kufareva, I., Khajehali, E., Cook, A. E., Abagyan, R., Conigrave, A. D., Sexton, P. M., Christopoulos, A., 2016. Towards a structural understanding of allosteric drugs at the human calcium-sensing receptor. Cell Res. 26(5), 574-92. https://doi.org/10.1038/cr.2016.36.

Lee, J., Rhee, M. H., Kim, E., & Cho, J. Y., 2012. BAY 11-7082 is a broad-spectrum inhibitor with anti-inflammatory activity against multiple targets. Mediators Inflamm. 2012, 416036. https://doi.org/10.1155/2012/416036.

Liang, T., Zhang, Y., Wu, S., Chen, Q., Wang, L., 2022. The Role of NLRP3 Inflammasome in Alzheimer's Disease and Potential Therapeutic Targets. Front. Pharmacol. 13, 845185. https://doi.org/10.3389/fphar.2022.845185.

Liddelow, S. A., Guttenplan, K. A., Clarke, L. E., Bennett, F. C., Bohlen, C. J., Schirmer, L., Bennett, M. L., Münch, A. E., Chung, W. S., Peterson, T. C., Wilton, D. K., Frouin, A., Napier, B. A., Panicker, N., Kumar, M., Buckwalter, M. S., Rowitch, D. H., Dawson, V. L., Dawson, T. M., Stevens, B., Barres, B. A., 2017. Neurotoxic reactive astrocytes are induced by activated microglia. Nature 541(7638), 481–487. https://doi.org/10.1038/nature21029

Liu, A. M., Lo, R. K., Wong, C. S., Morris, C., Wise, H., Wong, Y. H., 2006. Activation of STAT3 by G alpha(s) distinctively requires protein kinase A, JNK, and phosphatidylinositol 3-kinase. J. Biol. Chem. 281(47), 35812–25. https://doi.org/10.1074/jbc.M605288200.

Liu, Z., Wang, C., Yang, J., Chen, Y., Zhou, B., Abbott, D. W., Xiao, T. S., 2020. Caspase-1 Engages Full-Length Gasdermin D through Two Distinct Interfaces That Mediate Caspase Recruitment and Substrate Cleavage. Immunity 53(1), 106-114.e5. https://doi.org/10.1016/j.immuni.2020.06.007.

Lopez-Castejon, G., Luheshi, N. M., Compan, V., High, S., Whitehead, R. C., Flitsch, S., Kirov, A., Prudovsky, I., Swanton, E., Brough, D., 2013. Deubiquitinases regulate the activity of caspase-1 and interleukin-1β secretion via assembly of the inflammasome. J. Biol. Chem. 288(4), 2721-33. https://doi.org/10.1074/jbc.M112.422238.

López-Teros, M., Alarcón-Aguilar, A., Castillo-Aragón, A., Königsberg, M., Luna-López, A., 2024. Cytokine profiling in senescent and reactive astrocytes: A systematic review. Neurobiol. Aging 138, 28-35. https://doi.org/10.1016/j.neurobiolaging.2024.02.012.

Lye, J. J., Latorre, E., Lee, B. P., Bandinelli, S., Holley, J. E., Gutowski, N. J., Ferrucci, L., Harries, L. W. 2019. Astrocyte senescence may drive alterations in GFAPα, CDKN2A p14ARF, and TAU3 transcript expression and contribute to cognitive decline. GeroScience 41, 561–573. https://doi.org/10.1007/s11357-019-00100-3.

Ma, C., Li, S., Hu, Y., Ma, Y., Wu, Y., Wu, C., Liu, X., Wang, B., Hu, G., Zhou, J., Yang, S., 2021. AIM2 controls microglial inflammation to prevent experimental autoimmune encephalomyelitis. J. Exp. Med. 218(5), e20201796. https://doi.org/10.1084/jem.20201796.

Masters, C. L., Selkoe, D. J., 2012. Biochemistry of amyloid β-protein and amyloid deposits in Alzheimer disease. Cold Spring Harb. Perspect. Med. 2(6), a006262. https://doi.org/10.1101/cshperspect.a006262.

Mawuenyega, K. G., Sigurdson, W., Ovod, V., Munsell, L., Kasten, T., Morris, J. C., Yarasheski, K. E., Bateman, R. J., 2010. Decreased clearance of CNS beta-amyloid in Alzheimer's disease. Science 330(6012), 1774. https://doi.org/10.1126/science.1197623.

McKee CM, Coll RC. NLRP3 inflammasome priming: A riddle wrapped in a mystery inside an enigma. J Leukoc Biol. 2020 Sep;108(3):937-952. doi: 10.1002/JLB.3MR0720-513R. Epub 2020 Aug 3. PMID: 32745339.

Mészáros Á, Molnár, K., Fazakas, C., Nógrádi, B., Lüvi, A., Dudás, T., Tiszlavicz, L., Farkas, A. E., Krizbai, I. A., Wilhelm, I., 2023. Inflammasome activation in peritumoral astrocytes is a key player in breast cancer brain metastasis development. Acta Neuropathol. Commun. 11(1), 155. https://doi.org/10.1186/s40478-023-01646-2.

Minkiewicz, J., de Rivero Vaccari, J. P., Keane, R. W., 2013. Human astrocytes express a novel NLRP2 inflammasome. Glia 61(7), 1113–21. https://doi.org/10.1002/glia.22499.

Moonen, S., Koper, M. J., Van Schoor, E., Schaeverbeke, J. M., Vandenberghe, R., von Arnim, C. A. F., Tousseyn, T., De Strooper, B., Thal, D. R., 2023. Pyroptosis in Alzheimer's disease: cell type-specific activation in microglia, astrocytes and neurons. Acta Neuropathol. 145(2), 175-195. https://doi.org/10.1007/s00401-022-02528-y.

Nemeth, E.F., 2002.The search for calcium receptor antagonists (calcilytics). J. Mol. Endocrinol., 29, 15-21. https://doi.org/10.1677/jme.0.0290015.

Nielsen, H. M., Veerhuis, R., Holmqvist, B., Janciauskiene, S., 2009. Binding and uptake of A beta1-42 by primary human astrocytes in vitro. Glia 57(9), 978-88. https://doi.org/10.1002/glia.20822.

Nygaard, H. B., Strittmatter, S. M., 2009. Cellular prion protein mediates the toxicity of β-amyloid oligomers. Implications for Alzheimer disease. Arch. Neurol. 66(11), 1325–8. https://doi.org/10.1001/archneurol.2009.223.

Orduña-Castillo, L. B., Del-Río-Robles, J. E., García-Jiménez, I., Zavala-Barrera, C., Beltrán-Navarro, Y. M., Hidalgo-Moyle, J. J., Ramírez-Rangel, I., Hernández-Bedolla, M. A., Reyes-Ibarra, A. P., Valadez-Sánchez, M., et al., 2022. Calcium sensing receptor stimulates breast cancer cell migration via the Gβγ-AKT-mTORC2 signaling pathway. J. Cell Commun. Signal. 16(2), 239-52. https://doi.org/10.1007/s12079-021-00662-y.

Pacchiana, R., Abbate, M., Armato, U., Dal Prà, I., Chiarini, A., 2014. Combining immunofluorescence with in situ proximity ligation assay: a novel imaging approach to monitor protein-protein interactions in relation to subcellular localization. Histochem. Cell Biol. 42(5), 593-600. https://doi.org/10.1007/s00418-014-1244-8.

Pelletier, S., Duhamel, F., Coulombe, P., Popoff, M. R., Meloche, S., 2003. Rho family GTPases are required for activation of Jak/STAT signaling by G protein-coupled receptors. Mol. Cell. Biol. 23(4), 1316–33. https://doi.org/10.1128/MCB.23.4.1316-1333.2003.

Pike, C. J., Walencewicz-Wasserman, A. J., Kosmoski, J., Cribbs, D. H., Glabe, C. G., Cotman, C. W., 1995. Structure-activity analyses of beta-amyloid peptides: contributions of the beta 25-35 region to aggregation and neurotoxicity. J. Neurochem. 64(1), 253–265. https://doi.org/10.1046/j.1471-4159.1995.64010253.x.

Pippis, E. J., Yacyshyn, B. R., 2021. Clinical and Mechanistic Characteristics of Current JAK Inhibitors in IBD. Inflamm. Bowel Dis. 27(10), 1674–83. https://doi.org/10.1093/ibd/izaa318.

Plant, L.D., Boyle, J. P., Smith, I. F., Peers, C., Pearson, H. A., 2003. The production of amyloid beta peptide is a critical requirement for the viability of central neurons. J Neurosci. 23(13), 5531–5. https://doi.org/10.1523/JNEUROSCI.23-13-05531.2003.

Puzzo, D., Privitera, L., Leznik, E., Fà, M., Staniszewski, A., Palmeri, A., Arancio, O., 2008. Picomolar amyloid-beta positively modulates synaptic plasticity and memory in hippocampus. J. Neurosci. 28(53), 14537–45. https://doi.org/10.1523/JNEUROSCI.2692-08.2008.

Qin, H., Buckley, J. A., Li, X., Liu, Y., Fox, T. H. 3rd, Meares, G. P., Yu, H., Yan, Z., Harms, A. S., Li, Y., Standaert, D. G., Benveniste, E. N., 2016. Inhibition of the JAK/STAT Pathway Protects Against α-Synuclein-Induced Neuroinflammation and Dopaminergic Neurodegeneration. J. Neurosci. 36(18), 5144–59. https://doi.org/10.1523/JNEUROSCI.4658-15.2016.

Riccardi, D., Kemp, P. J., 2012. The calcium-sensing receptor beyond extracellular calcium homeostasis: conception, development, adult physiology, and disease. Annu. Rev. Physyiol. 74, 271–97. https://doi.org/10.1146/annurev-physiol-020911-153318.

Ries, M., Sastre, M., 2016. Mechanisms of Aβ clearance and degradation by glial cells. Front. Aging Neurosci. 8, 1–9. https://doi.org/10.3389/fnagi.2016.00160.

Ritorto, M. S., Ewan, R., Perez-Oliva, A. B., Knebel, A., Buhrlage, S. J., Wightman, M., Kelly, S. M., Wood, N. T., Virdee, S., Gray, N. S., et al., 2014. Screening of DUB activity and specificity by MALDI-TOF mass spectrometry. Nat. Commun. 5, 4763. https://doi.org/10.1038/ncomms5763.

Roberts, B. R., Lind, M., Wagen, A. Z., Rembach, A., Frugier, T., Li, Q. X., Ryan, T. M., McLean, C. A., Doecke, J. D., Rowe, C. C., Villemagne, V. L., & Masters, C. L., 2017. Biochemically-defined pools of amyloid-β in sporadic Alzheimer's disease: correlation with amyloid PET. Brain 140(5), 1486–1498. https://doi.org/10.1093/brain/awx057

Rossol, M., Pierer, M., Raulien, N., Quandt, D., Meusch, U., Rothe, K., Schubert, K., Schöneberg, T., Schaefer, M., Krügel, U., Smajilovic, S., Bräuner-Osborne, H., Baerwald, C., Wagner, U., 2012. Extracellular Ca2+ is a danger signal activating the NLRP3 inflammasome through G protein-coupled calcium sensing receptors. Nat. Commun. 3, 1329. https://doi.org/10.1038/ncomms2339.

Royston, P., 1995. Remark AS R94: A Remark on Algorithm AS 181: The W-test for Normality. Journal of the Royal Statistical Society. Series C (Applied Statistics) 44(4), 547–551. https://doi.org/10.2307/2986146.

Rybchyn, M. S., Islam, K. S., Brennan-Speranza, T. C., Cheng, Z., Brennan, S. C., Chang, W., Mason, R. S., & Conigrave, A. D., 2019. Homer1 mediates CaSR-dependent activation of mTOR complex 2 and initiates a novel pathway for AKT-dependent β-catenin stabilization in osteoblasts. J. Biol. Chem. 294(44), 16337–50. https://doi.org/10.1074/jbc.RA118.006587.

Salas-Venegas, V., Santín-Márquez, R., Ramírez-Carreto, R. J., Rodríguez-Cortés, Y. M., Cano-Martínez, A., Luna-López, A., Chavarría, A., Konigsberg, M., López-Díazguerrero, N. E., 2023. Chronic consumption of a hypercaloric diet increases neuroinflammation and brain senescence, promoting cognitive decline in middle-aged female Wistar rats. Front. Aging Neurosci. 15, 1162747. https://doi.org/10.3389/fnagi.2023.1162747.

Salminen, A., Ojala, J., Kaarniranta, K., Haapasalo, A., Hiltunen, M., & Soininen, H., 2011. Astrocytes in the aging brain express characteristics of senescence-associated secretory phenotype. Eur. J. Neurosci. 34(1), 3-11. https://doi.org/10.1111/j.1460-9568.2011.07738.x.

Selkoe, D. J., Hardy, J., 2016. The amyloid hypothesis of Alzheimer's disease at 25 years. EMBO Mol. Med. 8(6), 595-608. https://doi.org/10.15252/emmm.201606210.

Shaked, G. M., Kummer, M. P., Lu, D. C., Galvan, V., Bredesen, D. E., Koo, E. H., 2006. Abeta induces cell death by direct interaction with its cognate extracellular domain on APP (APP 597-624). FASEB J. 20, 1254–56. https://doi.org/10.1096/fj.05-5032fje.

Shankar, G. M., Bloodgood, B. L., Townsend, M., Walsh, D. M., Selkoe, D. J., Sabatini, B. L., 2007. Natural oligomers of the Alzheimer amyloid-beta protein induce reversible synapse loss by modulating an NMDA-type glutamate receptor-dependent signaling pathway. J. Neurosci. 27, 2866–75. https://doi.org/10.1523/JNEUROSCI.4970-06.2007.

Silve, C., Petrel, C., Leroy, C., Bruel, H., Mallet, E., Rognan, D., Ruat, M., 2005. Delineating a Ca2+ binding pocket within the Venus flytrap module of the human calcium-sensing receptor. J. Biol. Chem. 280(45), 37917-23. https://doi.org/10.1074/jbc.M506263200.

Simmnacher, K., Krach, F., Schneider, Y., Alecu, J. E., Mautner, L., Klein, P., Roybon, L., Prots, I., Xiang, W., Winner, B., 2020. Unique signatures of stress-induced senescent human astrocytes. Exp. Neurol. 334, 113466. https://doi.org/10.1016/j.expneurol.2020.113466.

Smith, A. M., Davey, K., Tsartsalis, S., Khozoie, C., Fancy, N., Tang, S. S., Liaptsi, E., Weinert, M., McGarry, A., Muirhead, R. C. J., et al., 2022. Diverse human astrocyte and microglial transcriptional responses to Alzheimer's pathology. Acta Neuropathol. 143(1), 75–91. https://doi.org/10.1007/s00401-021-02372-6.

Söderberg O, Gullberg, M., Jarvius, M., Ridderstråle, K., Leuchowius, K. J., Jarvius, J., Wester, K., Hydbring, P., Bahram, F., Larsson, L. G., Landegren, U., 2006. Direct observation of individual endogenous protein complexes in situ by proximity ligation. Nat. Methods 3(12), 995-1000. https://doi.org/10.1038/nmeth947.

Sun, X., Song, X., Zhang, L., Sun, J., Wei, X., Meng, L., An, J., 2016. NLRP2 is highly expressed in a mouse model of ischemic stroke. Biochem. Biophys. Res. Commun. 479, 656–62. https://doi.org/10.1016/j.bbrc.2016.09.157

Tfelt-Hansen, J., Chattopadhyay, N., Yano, S., Kanuparthi, D., Rooney, P., Schwarz, P., Brown, E. M., 2004. Calcium-sensing receptor induces proliferation through p38 mitogen-activated protein kinase and phosphatidylinositol 3-kinase but not extracellularly regulated kinase in a model of humoral hypercalcemia of malignancy. Endocrinology145(3), 1211–17. https://doi.org/10.1210/en.2003-0749.

Thoreen, C. C., Kang, S. A., Chang, J. W., Liu, Q., Zhang, J., Gao, Y., Reichling, L. J., Sim, T., Sabatini, D. M., Gray, N. S, 2009. An ATP-competitive mammalian target of rapamycin inhibitor reveals rapamycin-resistant functions of mTORC1. J. Biol. Chem. 284(12), 8023-32. https://doi.org/10.1074/jbc.M900301200.

Truvé, K., Parris, T.Z., Vizlin-Hodzic, D., Salmela, S., Berger, E., Ågren, H., and Funa, K., 2020. Identification of candidate genetic variants and altered protein expression in neural stem and mature neural cells support altered microtubule function to be an essential component in bipolar disorder. Transl. Psychiatry 10, 390. https://doi.org/10.1038/s41398-020-01056-1.

Ungerleider, K., Beck, J., Lissa, D., Turnquist, C., Horikawa, I., Harris, B. T., Harris, C. C., 2021. Astrocyte senescence and SASP in neurodegeneration: tau joins the loop. Cell Cycle 20(8), 752-764. https://doi.org/10.1080/15384101.2021.1909260.

Vizlin-Hodzic, D., Zhai, Q., Illes, S., Södersten, K., Truvé, K., Parris, T. Z., Sobhan, P. K., Salmela, S., Kosalai, S. T., Kanduri, C., Strandberg, J., Seth, H., Bontell, T. O., Hanse, E., Ågren, H., and Funa, K., 2017. Early onset of inflammation during ontogeny of bipolar disorder: the NLRP2 inflammasome gene distinctly differentiates between patients and healthy controls in the transition between iPS cell and neural stem cell stages. Transl. Psychiatry 7, e1010. https://doi.org/10.1038/tp.2016.284

Walsh, J. G., Muruve, D. A., Power, C., 2014. Inflammasomes in the CNS. Nat Rev Neurosci. 15(2), 84-97. https://doi.org/10.1038/nrn3638.

Ward, B. K., Magno, A. L., Walsh, J. P., Ratajczak, T., 2012. The role of the calcium-sensing receptor in human disease. Clin. Biochem. 45(12), 943-953. https://doi.org/10.1016/j.clinbiochem.2012.03.034.

Wu, P. J., Liu, H. Y., Huang, T. N., Hsueh, Y. P., 2016. AIM 2 inflammasomes regulate neuronal morphology and influence anxiety and memory in mice. Sci. Rep. 6, 32405. https://doi.org/10.1038/srep32405.

Yano, S., Brown, E. M., Chattopadhyay, N., 2004. Calcium-sensing receptor in the brain. Cell Calcium 35(3), 257–64. https://doi.org/10.1016/j.ceca.2003.10.008.

Yang, Y., Lang, X., Sun, S., Gao, C., Hu, J., Ding, S., Li, J., Li, Y., Wang, F., Gong, T., 2018. NLRP2 negatively regulates antiviral immunity by interacting with TBK1. Eur. J. Immunol. 48:1817–25. https://doi.org/10.1002/eji.201847589.

Zhang, M., Wu, Y., Gao, R., Chen, X., Chen, R., Chen, Z., 2022. Glucagon-like peptide-1 analogs mitigate neuroinflammation in Alzheimer's disease by suppressing NLRP2 activation in astrocytes. Mol. Cell. Endocrinol. 542, 111529. https://doi.org/10.1016/j.mce.2021.111529.

Zhang, Q., Sun, Y., He, Z., Xu, Y., Li, X., Ding, J., Lu, M., & Hu, G., 2020. Kynurenine regulates NLRP2 inflammasome in astrocytes and its implications in depression. Brain Behav. Immun. 88, 471–481. https://doi.org/10.1016/j.bbi.2020.04.016.

Zhang, X., Hong, S., Qi, S., Liu, W., Zhang, X., Shi, Z., Chen, W., Zhao, M., Yin, X., 2019. NLRP3 Inflammasome is involved in Calcium-Sensing Receptor-induced aortic remodeling in SHRs. Mediators Inflamm. 2019, 6847087. https://doi.org/10.1155/2019/6847087.

Zhao, W. Q., De Felice, F. G., Fernandez, S., Chen, H., Lambert, M. P., Quon, M. J., Krafft, G. A., & Klein, W. L., 2008. Amyloid beta oligomers induce impairment of neuronal insulin receptors. FASEB J. 22, 246–60. https://doi.org/10.1096/fj.06-7703com.

Zlokovic, B. V., Deane, R., Sagare, A. P., Bell, R. D., Winkler, E. A., 2010. Low-density lipoprotein receptor-related protein-1: a serial clearance homeostatic mechanism controlling Alzheimer's amyloid β-peptide elimination from the brain. J. Neurochem. 115(5), 1077-89. https://doi.org/10.1111/j.1471-4159.2010.07002.x.

Figure Legends

Fig. 1 Exogenous soluble or fibrillar $A\beta_{25-35}$ forms complexes with the ECDs (aka *Venus's flytraps*) of HCAs' CaSRs, whose intracellular signals induce, besides other effects (see Fig. 10 for details), the *de novo* synthesis and intracellular accumulation of endogenous $A\beta_{42}$-os. **A.** The *is*PLA analysis did not reveal any spots in untreated (Ctr) HCAs **(a-c)**. In contrast, the analysis revealed specific $A\beta_{25-35}$•CaSR complexes formed at the plasma membranes of cultured nonpermeabilized $A\beta_{25-35}$-treated HCAs (**d-f**). In **a** and **d**, separated pictures of DAPI-stained nuclei are shown, while in **b** and **e**, separate pictures of the plasmalemma outer surface are visualized. In **b**, no spot is visible, while, in **e**, the $A\beta_{25-35}$•CaSR complexes appear as red dots of varying sizes (from *puncta* to patches). In **c**, the merged **a** and **b** IF pictures of Ctr show nuclei in cyan and the absence of any red dots. In **f**, the merged **d** and **e** IF pictures of soluble $A\beta_{25-35}$-treated HCAs show $A\beta_{25-35}$•CaSR complexes in red and nuclei in cyan. **B.** *Left panel*: *is*PLA picture of a single nonpermeabilized HCA at a higher magnification. The *is*PLA signals (red) reveal that after 15-min exposure to 5.0 μM exogenous soluble biotinylated $A\beta_{25-35}$, $A\beta_{25-35}$•CaSR complexes have formed as *puncta* and patches of varied sizes at the outer surface of the plasma membrane. Nuclear DNA, cyan. *Right panel*: The 3D MIP-rendering of the same nonpermeabilized HCA as in the left panel seen in an oblique lateral projection. The location of the $A\beta_{25-35}$•CaSR complexes (red color) at the plasmalemma outer surface is clearly visible. **C.** *Left Panel*: Untreated HCAs (Ctr) do not produce any amounts of $A\beta_{42}$ detectable by standard IF. *Right panel*. HCAs treated with

exogenous fibrillar $A\beta_{25-35}$ (fuchsia) show fine aggregates of endogenous $A\beta_{42}$-os (green) in their cytosol. Nuclei were stained with DAPI (blue). For technical details, please refer to Materials and Methods and to (Pacchiana et al., 2014). These pictures are representative of ten distinct experiments. f$A\beta_{25-35,}$ fibrillar $A\beta_{25-35}$; $A\beta_{42}$-os, $A\beta_{42}$-oligomers.

Fig. 2 The signals from Aβ•CaSR complexes drive the early (at 1-h) phospho-activation of components of Akt/mTOR/AMPKα axis (**A**) and TYK2/JAK/STAT axis (**B**) in HCAs. Signaling pathway-specific membrane-based double-antibody arrays (details in Materials and Methods) were challenged with equal amounts of total protein lysates from Ctr, Aβ- or Aβ+NPS2143-treated HCAs to assess any difference in specific activating phosphorylation sites of different proteins. A 30-min pretreatment with calcilytic NPS2143 effectively blocked these enzymatic phospho-activations by Aβ•CaSR signals. The integrated intensity values for each couple of specific protein spots and their levels of statistical significance are mean values ± standard deviations (SDs) of 3 distinct experiments. The superimposed "k" shows that actual values are in thousands (= k). The statistical analysis was conducted using one-way ANOVA followed by Dunnett's *post-hoc* test: *, $p < 0.05$; **, $p < 0.01$; ***, $p < 0.001$.

Fig. 3 The signals from HCAs' Aβ•CaSR complexes drive the early *NLRP2* mRNA and NLRP2 PRR protein overexpression but do not affect the latter's next slow decline. **A**. *NLRP2* transcript levels assessed by RT-qPCR in untreated controls (Ctr) and after 1-h-exposure to $A\beta_{25-35}$ ± NPS2143. The data are means ± SE of CNRQ values from 3 distinct experiments with Ctr values normalized to 1.0. **B**. *Top panel*: Typical immunoblot showing the NLRP2 PRR protein expression changes *vs*. untreated Ctr according to the experimental treatments. LC, loading control (i.e., β-actin). *Bottom panel:* Densitometric assessments of NLRP2 PRR protein bands in the immunoblots for each time point and experimental treatment, expressed as integral intensity values. The data are means ± SD of 3 distinct experiments with Ctr values normalized to 1.0. Statistical analysis was conducted using one-way ANOVA followed by Dunnett's *post-hoc* test. Pair-wise comparisons were made between the corresponding $A\beta_{25-35}$ ± NPS2143 treatments at each time point: *, $p < 0.05$. Comparisons of each treated group *vs*. 0-h Ctr: #, $p < 0.01$ at least.

Fig. 4 The signals from HCAs' Aβ•CaSR complexes drive the early *NLRP3* mRNA and NLRP3 PRR protein overexpression, yet they do not affect the latter's later slow decline. **A**. *Top panel*: *NLRP3* transcript levels figured out by RT-qPCR detected in controls (Ctr) and after 1h-exposure to $A\beta_{25-35}$ ± NPS2143. The data are means ± SE of CNRQ values from 3 distinct experiments with Ctr values normalized to 1.0. **B**. *Top panel*: Changes in NLRP3 PRR protein expression occurred in the treated samples compared to untreated controls (Ctr), as shown in a typical immunoblot. LC, Loading control, i.e., β-actin. *Bottom panel:* The graph displays the densitometric evaluations of NLRP3 PRR protein bands in the immunoblots for each time point and experimental treatment, expressed as integral intensity values. Data are means ± SD of 3 distinct experiments with Ctr values normalized to 1.0; they were statistically analyzed using one-way ANOVA followed by Dunnett's *post-hoc* test: pair-wise comparisons between corresponding $A\beta_{25-35}$ ± NPS2143 treatments at each time point: **, $p < 0.01$; ****, $p < 0.0001$; comparisons of each treated group versus 0-h Ctr: #, $p < 0.01$ at least.

Fig. 5 The Aβ•CaSR complexes' signals rapidly suppress *AIM2* mRNA and AIM2 PRR protein expression in HCAs. **A**. *AIM2* transcript levels were assessed by RT-qPCR in controls (Ctr) and after 1-h exposure to $A\beta_{25-35}$ ± NPS2143. The data are means ± SE of CNRQ values from 3 distinct experiments with Ctr values normalized to 1.0. **B**. *Top panel*: Changes in AIM2 PRR protein expression based on the experimental treatments compared to untreated controls (Ctr) as seen in typical immunoblots. LC, loading control, i.e., β-actin. The samples derived from the same experiment and the gels/blots were processed in parallel. *Bottom panel:* The graph displays the densitometric evaluations of AIM2 PRR protein bands in the immunoblots for each time point

and experimental treatment, expressed as integral intensity values. The data are means ± SD of 3 distinct experiments with Ctr values normalized to 1.0; they were statistically analyzed using one-way ANOVA followed by Dunnett's *post-hoc* test: pair-wise comparisons between corresponding $A\beta_{25–35}$ ± NPS2143 treatments at each time point: **, $p < 0.01$; ****, $p < 0.0001$; comparisons of each treated group *vs*. 0-h Ctr: #, $p < 0.05$.

Fig. 6. The divergent regulations of NLRP2 and NLRP3 PRR protein levels on the one hand and of AIM2 PRR protein on the other hand as driven by 1-h-exposure to $A\beta_{25–35}$ by itself and by $A\beta_{25-35}$ added after a short pretreatment (30 min) with specific inhibitors of components of the JAK1-2/TYK2/STATs axis and the PI3K/Akt/mTOR/AMPKα axis. *Left side:* Typical immunoblots showing the changes of NLRP2 (**A**), NLRP3 (**B**), and AIM2 (**C**) PRR protein expressions *vs*. untreated Ctr according to the experimental treatments. LC, loading control (i.e., β-actin). *Middle:* The graphs show the densitometric assessments of NLRP2 (**A**), NLRP3 (**B**), and AIM2 (**C**) PRR protein bands in the immunoblots for each time point and experimental treatment, expressed as integral intensity values. The data are means ± SD of 3 distinct experiments with Ctr values normalized to 1.0. The results were statistically analyzed using one-way ANOVA followed by Dunnett's *post-hoc* test. The various treatments and corresponding levels of significance *vs*. Ctr or *vs*. Aβ are reported in the tables on the right side. Abbreviations: *BAY*, BAY 11-7082 (inhibitor of IκBα phosphorylation, NF-κB signaling, and ubiquitin-specific proteases USP7 and USP21); *BPC*, Brepoticinib P-Tosylate (TYK2, JAK1, and JAK2 inhibitor); *DOR*, Dorsomorphin (AMPKα inhibitor); *TOR*, Torin 1 (mTOR inhibitor); *LY*, LY294002 (PI3K inhibitor); ns, not significant.

Fig. 7 *PYCARD*/ASC expression in untreated (Ctr) and $A\beta_{25-35}$ ± NPS2143 exposed HCAs. **A**. Transcript levels of *PYCARD* gene figured out by RT-qPCR as detected after 1-h exposure to $A\beta_{25–35}$ ± NPS2143. The data are means ± SE of CNRQ values from 3 distinct experiments with Ctr values normalized to 1.0. **B**. Typical immunoblots showing the changes of ASC protein expression *vs*. untreated controls according to the experimental treatments. LC, loading control (i.e., β-actin). The samples were derived from the same experiment, and the gels/blots were processed in parallel. The graph shows the densitometric assessments of ASC protein bands in the immunoblots for each time point and experimental treatment, expressed as integral intensity values. The data are means ± SD of 3 distinct experiments with Ctr values normalized to 1.0; they were statistically analyzed using one-way ANOVA followed by Dunnett's *post-hoc* test. Pair-wise comparisons between the corresponding $A\beta_{25–35}$ ± NPS2143 treatments at each time point: *, $p < 0.05$; **, $p < 0.01$; comparisons of each treated group versus 0-h Ctr: #, $p < 0.05$.

Fig. 8 Effects on Caspase 1 and Caspase 4 in HCAs exposed to $A\beta_{25-35}$ ± NPS2143. *CASP1* (**A**) and *CASP4* (**F**) transcript levels as assessed by RT-qPCR after 1-h exposure to $A\beta_{25–35}$ ± NPS2143. The data are means ± SE of CNRQ values from 3 distinct experiments with Ctr values normalized to 1.0. Densitometric evaluations of specific bands of Procaspase 1 (50 kDa) (**B**) and its P20 fragment (**C**), and of Procaspase 4 (**G**) in the immunoblots for each time point and experimental treatment, expressed as integral intensity values. The data are means ± SD of 3 distinct experiments with Ctr values normalized to 1.0. Typical immunoblot revealing Procaspase 1 (50kDa) and its P20 fragment (**D**), and Procaspase 4 (**H**) expression according to experimental treatments *vs*. Ctr. LC, loading control (i.e., β-actin). Note that no specific Caspase 4 P20 fragment is visible. Caspase 1 (**E**) and Caspase 4 (**I**) enzymatic activities were assayed on whole HCAs protein extracts after exposure to $A\beta_{25–35}$ ± NPS2143, as described in Materials and Methods. Points in the curves are means ± SD of 3 independent experiments, expressed as arbitrary units corresponding to $\Delta F\ \mu g^{-1}$ protein of each experimental group. Statistical analysis of the data was conducted using one-way ANOVA followed by Dunnett's *post-hoc* test. Pair-wise comparisons between corresponding $A\beta_{25–35}$ ± NPS2143 treatments at each time point: *, $p < 0.05$; **, $p < 0.01$; ***, $p < 0.001$; ****, $p < 0.0001$; comparisons of each treated group versus 0-h CTR: #, $p < 0.05$.

Fig. 9 Effects of the signals from Aβ•CaSR complexes on *IL1B* and *GSDMD* mRNAs and corresponding protein levels in HCAs. (**A)**: *IL1B* transcript levels detected by RT-qPCR after 1-h exposure to $A\beta_{25–35}$ ± NPS2143. The data are means ± SE of CNRQ values from 3 distinct experiments with Ctr values normalized to 1.0. (**B**): *Bottom panel:* Typical immunoblots showing IL-1β precursor protein expression levels in $A\beta_{25–35}$ ± NPS2143 treated *vs*. untreated controls (Ctr). LC, loading control (i.e., β-actin). *Top panel:* Densitometric assessments of IL-1β precursor protein bands in the immunoblots for each time point and experimental treatment, expressed as integral intensity values. (**C**): *GSDMD* transcript levels found by RT-qPCR detected in Ctr and $A\beta_{25–35}$ ± NPS2143 treated samples. The data are means ± SE of CNRQ values from 3 distinct experiments with Ctr values normalized to 1.0. (**D)**: *Bottom panel:* Typical immunoblots showing the levels of Gasdermin D holoprotein expression *vs*. untreated controls (Ctr) according to the experimental treatments expressed as integral intensity values. No bands of Gasdermin D N-terminal fragments are detectable. LC, loading control (i.e., β-actin). The samples were derived from the same experiment, and the gels/blots were processed in parallel. *Top panel:* Densitometric assessments of Gasdermin D precursor protein bands in the immunoblots for each time point and experimental treatment. The data are means ± SD of 3 independent experiments, with 0-h values normalized as 1.0; they were statistically analyzed using one-way ANOVA followed by Dunnett's *post-hoc* test. Significant differences between mRNA mean CNRQ values are pointed out with: *, $p < 0.05$; **, $p < 0.01$; ***, $p < 0.001$; ****, $p < 0.0001$.

Fig. 10 Graphical summary of the manifold neurotoxic and pro-inflammatory effects driven by Aβ•CaSR signals in HCAs. Most importantly, calcilytic (or CaSR NAM) NPS2143 given as a short (30-min) pretreatment, totally prevented (or significantly mitigated in the case of RANTES, MCP2, and sICAM1 only) all the shown harmful effects brought about by Aβ•CaSR signals in HCAs while restoring the nonamyloidogenic metabolism of APP and the release of neurotrophic and neuroprotective sAPPα. Thus, calcilytics would hinder the self-sustained spreading of the main drivers of AD's neuropathology, neuroinflammation, death of neurons and oligodendrocytes, and connectome damage. For further details, see the text and references (Armato et al., 2013; Chiarini et al., 2017a, 2017b, 2020b; Dal Prà et al., 2005, 2014a, 2014b; Gardenal et al., 2017).

HIGHLIGHTS

- Aβ•CaSR complexes quickly assemble at HCAs' plasma membrane.
- Aβ•CaSR signals activate PI3K/Akt/mTOR/AMPKα and TYK2/JAK/STATs axes.
- Aβ•CaSR signals upregulate NLRP2 and NLRP3 PRRs yet downregulate AIM2 PRR.
- CaSR negative allosteric modulator NPS2143 specifically hinders the above effects.
- Aβ•CaSR signals are an inflammasomal first priming but not a second signal in HCAs